

*Review Article*

# Photodoping Effects in High Critical Temperature Superconducting Films and Josephson Junctions

A. Gilabert,<sup>1</sup> A. Hoffmann,<sup>2,3</sup> M. G. Medici,<sup>1</sup> and I. K. Schuller<sup>2</sup>

*Received 25 May 1999*

---

Persistent photoconductivity is an interesting and unusual property of high temperature superconductors. Illumination of these compounds can lead to a change in doping that is persistent at low temperature and relaxes back to its initial value at elevated temperatures. This photodoping can give rise to an improvement of superconducting properties, which is contrary to the illumination effects in conventional superconductors. Furthermore, these photo-induced effects can also be used to probe and modify the properties of grain boundaries in grain boundary Josephson junctions. This paper reviews the experimental data and proposed theoretical models related to these photoinduced effects.

---

**KEY WORDS:** Doping; Josephson junctions; photoconductivity; superconductivity; thin films.

## 1. INTRODUCTION

The interaction of light with conventional superconductors was mainly focused on during the 1970's. Photons, which have energies larger than the binding energy  $2\Delta$  of the Cooper pairs, are able to break the superconducting carriers and create quasiparticles, which recombine with the emission of phonons [1]. This results in an excess of quasiparticles compared to the normal concentration of thermally excited quasiparticles. This excess of quasiparticles corresponds to a higher effective temperature or to a smaller energy gap. Thus, visible light weakens the superconducting properties and the energy gap of illuminated samples has been shown to decrease proportionally to this excess density of quasiparticles (not too far from equilibrium) [2]. During the 1970's, many experiments were performed with classical superconductors submitted

not only to light but also to injection of electrons or phonons [for a review see Refs. 3, 4]. These experiments were interesting due to both fundamental and applied aspects. Different characteristic times such as quasiparticle recombination [5], gap relaxation [6,7], pair breaking, and the phonons escape times were determined and studied theoretically to set the time scale for nonequilibrium phenomena [8]. Theoretical predictions imply that a superconductor, driven out of equilibrium by external perturbations, may become unstable and undergo a transition to a nonequilibrium state or to the normal state [9]. Describing the nature of this transition and the final state was one of the challenges faced by physicists involved in nonequilibrium superconductivity. Besides these fundamental aspects of nonequilibrium superconductivity, it was expected that the interaction of light with classical superconductors will result in devices combining the advantages of superconductor and optical technologies [see for example Ref. 10].

Since the discovery of high  $T_c$  superconductivity (HTSC) [11], much attention has been paid to the investigation of the influence of light on HTSC [see for example Refs. 12, 13]. Like for low  $T_c$  superconduc-

---

<sup>1</sup>L.P.M.C. UMR 6622 Université de Nice Sophia Antipolis, Parc Valrose 06108 Nice Cedex 02, France.

<sup>2</sup>University of California—San Diego, Physics Department 0350, 9500 Gilman Drive, La Jolla, California 92093-0350.

<sup>3</sup>Present address: Los Alamos National Laboratory, MS H805, Los Alamos, New Mexico 87545.

tors, the visible light can break Cooper pairs in  $\text{YBa}_2\text{Cu}_3\text{O}_7$  thin films on a short illumination subnanosecond time scale [14–16], and for small photon dose, smaller than  $10^{16}$  photon/cm<sup>2</sup> [17]. At a longer millisecond to hours illumination time scale with a typical  $10^{19}$ – $10^{23}$  photon/cm<sup>2</sup> photon dose being the relevant parameter, a surprising improvement of the superconducting properties takes place [18,19]. The superconducting transition temperature of an oxygen-deficient superconducting  $\text{YBa}_2\text{Cu}_3\text{O}_x$  thin film increases considerably with illumination and this photo-induced change persists after the light is switched off if the sample is kept at low temperatures (typically below 100 K). This long-term “persistent photoinduced superconductivity” (PPS) is more pronounced for oxygen-deficient thin film and vanishes for fully oxygenated  $\text{YBa}_2\text{Cu}_3\text{O}_7$ . In the normal state or for semiconducting or insulating  $\text{YBa}_2\text{Cu}_3\text{O}_x$  thin films, light increases substantially the conductivity leading to a persistent photoinduced conductivity (PPC) [19]. An insulating  $\text{YBa}_2\text{Cu}_3\text{O}_x$  thin film close to the metal–insulator transition ( $x \approx 6.4$ ) can even become superconducting by illumination [20]. These astonishing effects are related to the wide range of changes, which are due to doping of HTSC, which makes the interaction between light and HTSC more interesting than in classical superconductors. The enhanced superconducting or photoconducting properties relax toward the original properties for temperatures close to room temperature.

The photodoping effect can be used in  $\text{YBa}_2\text{Cu}_3\text{O}_x$  grain boundary Josephson junctions (GBJJ) as an efficient method to tune the Josephson coupling. In these GBJJ, the grain boundary that constitutes the barrier is a weak, oxygen-deficient superconducting region. Illumination changes the transport properties of the oxygen-deficient barrier, thus changing the Josephson coupling. The PPS results in an increased dc Josephson current [21] and shifts the voltage positions of the Fiske resonances (ac Josephson properties) [22]. The PPC also induces a decrease of the normal state resistance of the junction similar to earlier results found in light-sensitive tunnel junctions with a semiconducting CdS barrier layer separating classical superconductors like Pb, In, Al, or Sn [23–25].

In this paper we discuss these interesting properties of photodoping of HTSC. First we give a short description of the experimental conditions including a brief summary of the structure of  $\text{YBa}_2\text{Cu}_3\text{O}_x$  (Section 2). Then we describe the interaction of light on HTSC thin films (Section 3), followed by a possible theoretical explanation (Section 4), and end with the effect of illumination of  $\text{YBa}_2\text{Cu}_3\text{O}_x$  grain boundary Josephson junctions (Section 5).

## 2. EXPERIMENTAL CONDITIONS

### 2.1. Preparation of High $T_c$ Superconducting Thin Film and $\text{YBa}_2\text{Cu}_3\text{O}_x$ GBJJ

Because the penetration depth of visible light in high  $T_c$  superconductors is of the order of 100 nm, most of the illumination experiments on high  $T_c$  superconductors are done on thin films. The preparation of  $\text{R}\text{Ba}_2\text{Cu}_3\text{O}_x$  thin films ( $R = \text{Y}$  or rare earth) used in photoexcitation experiments have been widely described [26]. To obtain well-defined oxygen deficiency, a fully oxygenated  $\text{R}\text{Ba}_2\text{Cu}_3\text{O}_x$  thin film is annealed and cooled following the pressure-temperature oxygen phase diagram line [27]. The oxygen content is determined after treatment from the expansion of the  $c$ -axis parameter [28–30] or the critical temperature. High  $T_c$  superconductors other than  $\text{R}\text{Ba}_2\text{Cu}_3\text{O}_x$  were prepared in similar ways.

For the fabrication of GBJJ, a  $\text{YBa}_2\text{Cu}_3\text{O}_x$  thin film is deposited on a bicrystal substrate formed from the fusion of two  $\text{SrTiO}_3$  single crystals with misaligned crystal axes ( $24^\circ$  or  $37^\circ$ ). The Josephson weak link is formed from a constriction, which is patterned perpendicular to the grain boundary. This planar geometry of these GBJJ is very well suited for illumination.

### 2.2. Photoexcitation Experimental Setup

The samples are either immersed in liquid nitrogen or helium, in a helium flow, in vacuum, or inert gas. These experiments in different conditions show that no changes in oxygen stoichiometry or other artifacts are responsible for the PPC or PPS. The transport measurements are done with a standard four probe or Hall bar technique. For the study of GBJJ, the current-voltage characteristics  $I(V, H)$  at different magnetic fields  $H$ , are unaffected by several temperature cycles even after a very long time (several months). No trapped magnetic flux are observed for magnetic fields below a few Gauss and the experimental  $I(V, H)$  curves are perfectly reproducible. After one night of relaxation at room temperature in darkness, the illuminated GBJJ or  $\text{YBa}_2\text{Cu}_3\text{O}_x$  thin films recover their original properties before illumination. Repeated illumination and relaxation cycles give reproducible effects [31–33].

Several light sources (lasers, halogen lamps, and Hg-Xe lamps) were used to illuminate the samples through optical windows of the cryostat. For most of

the excitation measurements, a 70 W Hg-Xe lamp, a halogen lamp, or an Ar laser ( $\lambda = 514$  nm) were used with a typical power density at the sample surface up to  $1$  W/cm<sup>2</sup>. To determine the spectral dependence, Endo *et al.* [34] used a 1000 W Hg-Xe arc lamp with an infrared water filter to protect the sample and optics from excessive heating. They have investigated specific wavelengths in the range from 250 nm to 1100 nm by using interference band-pass filters with a bandwidth of 10 nm. Using this setup, the power density of monochromatic light ranged between 0.04 and several mW/cm<sup>2</sup>.

Using much larger optical power density (of the order of MW/cm<sup>2</sup>) can lead to another phenomenon, the “laser writing,” which is different from the PPC and PPS effects [35]. Laser writing decreases the oxygen content due to local heating caused by the laser beam on HTSC thin films. Consequently, the superconducting properties decrease and the film can even become semiconducting. This effect can be reversible and it is possible to restore the superconducting properties by reapplying the same laser beam in an oxygen atmosphere.

### 2.3. Structural Aspects of High $T_c$ Superconductors

Many HTSC are characterized by their multilayered structure with regular stacking of CuO<sub>2</sub> planes connected by “charge reservoir layers.” These CuO<sub>2</sub> layers play a major role in the mechanism of superconductivity. It is believed that the “charge reservoir” layers supply the CuO<sub>2</sub> planes with charge carriers. In YBa<sub>2</sub>Cu<sub>3</sub>O<sub>*x*</sub>, the “charge reservoir” layers are the CuO chains along the *b*-axis. For YBa<sub>2</sub>Cu<sub>3</sub>O<sub>*x*</sub> the principal way to change the CuO<sub>2</sub> doping is by modifying the charge reservoir layers, e.g., by changing the oxygen concentration *x* in the CuO chains. By decreasing the oxygen content *x* of YBa<sub>2</sub>Cu<sub>3</sub>O<sub>*x*</sub> samples, oxygen atoms are removed from the chain leaving oxygen vacancies, which may play an important role in the photodoping effect in this compound. The CuO chains are infinitely long in the fully oxygenated case ( $x = 7$ ). As the number of oxygen vacancies increases from  $x = 7$  to  $x = 6.4$ , the length of the CuO chains decreases preserving orthorhombic symmetry. At high oxygen deficiencies ( $6.0 < x < 6.4$ ), the sample undergoes an orthorhombic-tetragonal structural transition where the *a*- and *b*-axes become equivalent. For the tetragonal  $x = 6$  phase, no oxygen atoms are left in the chain planes. Thus by decreasing the oxygen content, the CuO chains shorten, their effec-

tiveness as a charge reservoir decreases and therefore the charge density of the CuO<sub>2</sub> planes decreases, diminishing drastically the superconducting properties of the YBa<sub>2</sub>Cu<sub>3</sub>O<sub>*x*</sub> sample. As a result the critical temperature  $T_c$  of YBa<sub>2</sub>Cu<sub>3</sub>O<sub>*x*</sub> thin films decreases as a function of the oxygen content *x* from  $T_c = 90$  K for  $x = 7$  down to an insulating behavior ( $T_c = 0$  K) for  $x \approx 6.4$ .

The main structural difference between YBa<sub>2</sub>Cu<sub>3</sub>O<sub>*x*</sub> and most other cuprates is that the latter have no CuO chains and thus are either tetragonal or less orthorhombic than YBa<sub>2</sub>Cu<sub>3</sub>O<sub>*x*</sub>. The charge reservoir is believed to be maintained by other structural layers, such as the TlO layers in Tl<sub>2</sub>Ba<sub>2</sub>CuO<sub>6+ $\delta$</sub> . Typically the carrier density in these compounds can be modified in two ways: by introducing interstitial oxygen into the structure (e.g., Tl<sub>2</sub>Ba<sub>2</sub>CuO<sub>6+ $\delta$</sub> , Bi<sub>2</sub>Sr<sub>2</sub>CaCu<sub>2</sub>O<sub>8+ $\delta$</sub> ) or by replacing some of the cations (e.g., Sr for La in La<sub>2-*y*</sub>Sr<sub>*y*</sub>CuO<sub>4</sub>, Y for Ca in Bi<sub>2</sub>Sr<sub>2</sub>Ca<sub>1-*y*</sub>Y<sub>*y*</sub>Cu<sub>2</sub>O<sub>8</sub>).

## 3. ILLUMINATION EXPERIMENTS

### 3.1. RBa<sub>2</sub>Cu<sub>3</sub>O<sub>*x*</sub>

#### 3.1.1. Basic Effect

PPC was found in YBa<sub>2</sub>Cu<sub>3</sub>O<sub>*x*</sub> thin films after long-time illumination by Kudinov *et al.* [18,19,36–40] and studied by different groups [20,41–46]. Nieva *et al.* [20] discovered an increase in the  $T_c$  of oxygen deficient YBa<sub>2</sub>Cu<sub>3</sub>O<sub>*x*</sub> thin films after illumination, which indicates a PPS. For a brief review on PPC and PPS in RBa<sub>2</sub>Cu<sub>3</sub>O<sub>*x*</sub> thin films see Hoffmann *et al.* [47,48]. As an example, Fig. 1 shows the resistivity as a function of temperature for an oxygen deficient YBa<sub>2</sub>Cu<sub>3</sub>O<sub>6.45</sub> film before illumination (solid line) and after 8 hours of illumination (dashed line) using a halogen lamp. Both the conductivity and the  $T_c$  increased after illumination. For the YBa<sub>2</sub>Cu<sub>3</sub>O<sub>6.45</sub> film in Fig. 1 the increase of  $T_c$  is in excess of 10 K. Several orders of magnitude changes of conductivity after illumination can be found depending on the oxygen content [50]. This excited state is stable if the sample is kept at low temperatures, typically below 100 K. Most measurements only measure the photoinduced enhancement of the dc conductivity. Lately Widder *et al.* [51] used infrared absorption to show that after illumination the conductivity is enhanced up to frequencies of approximately 1.4 eV. Kityik and Koliunko [44] showed that these photoinduced effects are

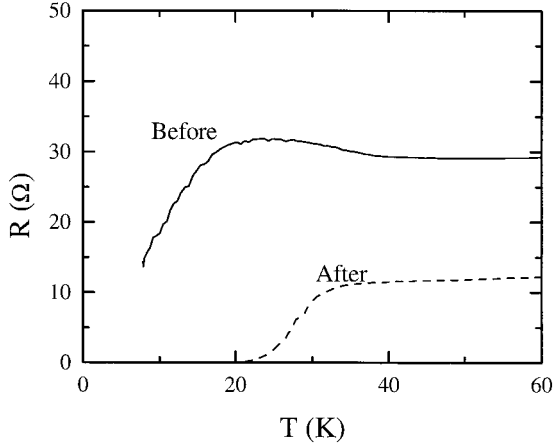


**Fig. 1.** Temperature dependence of the resistivity of oxygen deficient  $\text{GdBa}_2\text{Cu}_3\text{O}_{6.45}$  thin film before (solid line) and after (dashed line) illumination (adapted from Ref. 49).

not limited to thin films, but that they can also be observed in single crystals.

### 3.1.2. Time Dependence

Kudinov, Kirilyuk, and Kreines were the first to study the PPC relaxation in oxygen deficient  $\text{YBa}_2\text{Cu}_3\text{O}_x$  thin films [52]. Figure 2(b) shows the time dependence of the resistivity relaxation. The resistivity change is initially large and has a long, slowly

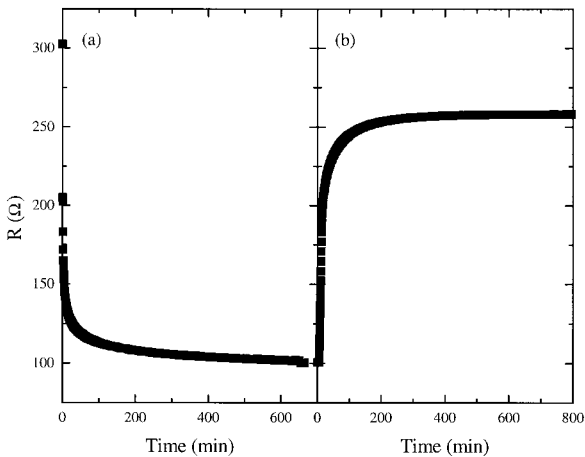


**Fig. 2.** Time dependence of the (a) excitation and (b) relaxation of persistent photoconductivity in a  $\text{GdBa}_2\text{Cu}_3\text{O}_{6.4}$  film. For the excitation, the light source was switched on at  $t = 0$ , while the sample was kept at 95 K. For the relaxation, the temperature was raised from 95 K to 300 K in about 12 min near  $t = 0$  (adapted from Ref. 49).

varying tail at large relaxation time. The resistivity relaxation  $\rho(t)$  as a function of relaxation time  $t$  can be described by a stretched exponential law [52]:

$$\rho(t) = \rho(\infty) + [\rho(0) - \rho(\infty)] \exp\left[-\left(\frac{t}{\tau}\right)^\beta\right], \quad (1)$$

where  $\rho(\infty)$  is the resistivity at full relaxation,  $\rho(0)$  the initial resistivity after illumination until saturation,  $\tau$  the relaxation time, and  $\beta$  a dimensionless dispersion parameter ( $0 \leq \beta \leq 1$ ).

This relaxation to the initial state can be as long as several hours at room temperature and more than 1200 h at 254 K [53–56]. Due to these long low-temperature relaxation times, the relaxation has no effect on the low temperature photodoping. The temperature dependence of  $\tau$  follows a thermal activation process:

$$\tau = \tau_0 \exp\left(\frac{\Delta}{k_B T}\right), \quad (2)$$

where  $\Delta$  is the energy barrier for relaxation and is found to be  $\Delta \approx 0.9 \pm 0.1$  eV [53–56]. This activation energy for the relaxation of the photoinduced effects is close to the oxygen diffusion activation energy of 1.3 eV [57]. This suggests that the photoinduced effects could be related to oxygen movement (see Section 4) and motivated several experiments, which are described in Section 3.1.7.

The time dependence of the photoexcitation is shown in Fig. 2(a). Although generally photoexcitation follows a stretched exponential behavior [similar to Eq. (1)] [34,55,56,58], Tanabe *et al.* [42] claimed a logarithmic time dependence. While the stretched exponential behavior for the *relaxation* can be explained by a distribution of relaxation times or energy barriers [53], the origin of this time dependence during *photoexcitation*, especially during monochromatic illumination, is not yet clear [34].

The photoexcitation time scales inversely with the intensity of the incident light [53], implying that the photoexcitation is a one-photon process. Therefore it is more meaningful to express the time dependence during photoexcitation in terms of the incident photon dose [34,53]:

$$n = \frac{I \times t}{\hbar\omega}, \quad (3)$$

where  $I$  is the incident light intensity,  $t$  the illumination time, and  $\hbar\omega$  the photon energy.

### 3.1.3. Transport Measurements

Information on the number of carriers can be obtained from measurements of the Hall coefficient  $R_H$  at fixed temperature versus illumination dose. The normal state resistivity  $\rho_{xx}$  [Fig. 3(a)] and the Hall coefficient  $R_H$  [Fig. 3(b)] show clearly the same illumination time dependence [41,46,59–64]. In a simple one-band model, the Hall coefficient is inversely proportional to the carrier density. Thus the data in Fig. 3 strongly suggest that, upon illumination, the carrier density increases, which results in a decrease of resistivity. Furthermore, the photoinduced change of  $T_c$  shows the same parabolic dependence on carrier concentration as observed for chemical doping [60].

In addition, the Hall mobility  $\mu = R_H/\rho_{xx}$  changes [Fig. 3(c)] and contributes to the variations in the resistivity [41,46,61–64]. At low temperatures  $\mu$  decreases with illumination, whereas at higher temperatures closer to room temperature  $\mu$  either increases

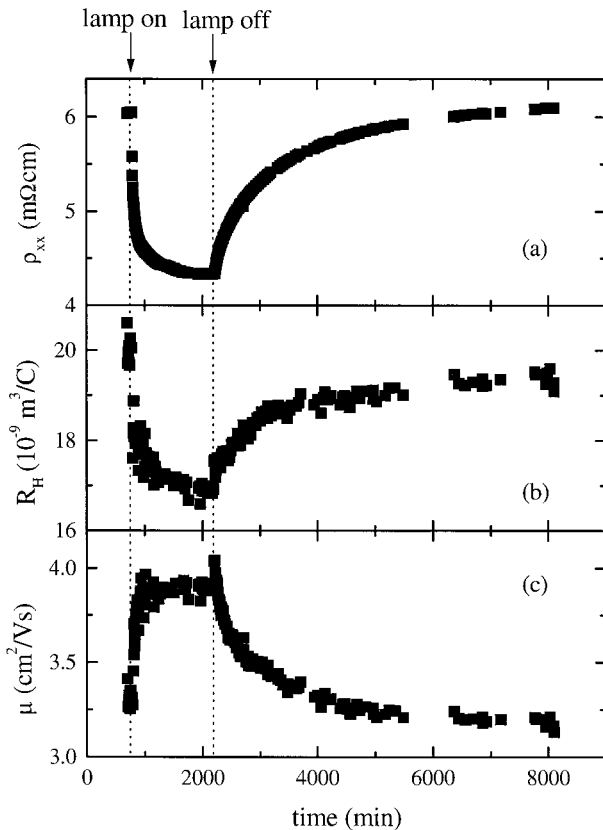


**Fig. 3.** Time dependence of the resistivity  $\rho$ , Hall coefficient  $R_H$ , and Hall mobility  $\mu = c(|R_H|/\rho)$  during excitation and relaxation measured at room temperature in a patterned  $\text{YBa}_2\text{Cu}_3\text{O}_{6.5}$  thin film (adapted from Ref. 41).

[41,46,62] or even shows a non-monotonic behavior with illumination [61,63,64]. This unusual temperature dependence of the photoinduced Hall mobility is distinct from the resistivity and Hall coefficient, which decrease with illumination at all temperatures. However, the meaning of  $\mu$  in a complex material like the cuprate superconductors is still controversial.

Dmitriev *et al.* showed that also the critical current density increases with illumination. Even highly doped films ( $x > 0.9$ ), with small changes in the normal state resistivity, exhibit pronounced enhancement of the critical current density [65–68].

Thick  $\text{RBa}_2\text{Cu}_3\text{O}_x$  films ( $\geq 400 \text{ \AA}$ ) show different time dependencies during excitation and relaxation [49] of the normal state properties (e.g.,  $\rho$ ) and the superconducting properties (e.g.,  $T_c$ ). This is probably caused by the finite light penetration depth together with the fact that  $\rho$  is given as an average across the film thickness, whereas  $T_c$  is a measure of the percolation path with the highest critical temperature. Interestingly, this hysteresis effect vanishes in *a*-axis oriented  $\text{RBa}_2\text{Cu}_3\text{O}_x$  films and in  $\text{GdBa}_2\text{Cu}_3\text{O}_x/\text{PrBa}_2\text{Cu}_3\text{O}_x$  superlattices [49]. Eremenko *et al.* [69,70] observed a similar result and explained this in terms of two distinct mechanisms leading to the persistent photoconductivity. However, this interpretation fails to explain the absence of hysteresis in thinner films.

To investigate the photoexcitation of the anisotropy, Markowitsch *et al.* [71] used  $\text{YBa}_2\text{Cu}_3\text{O}_{6.6}$  films grown on tilted  $\text{SrTiO}_3$  substrates (surface tilted  $10^\circ$  and  $20^\circ$  to the [001] direction) to separate the conductivity along the *ab*-plane and the *c*-axis. Photoexcitation enhanced the metallic conductivity in the *ab*-plane and the insulating one along the *c*-axis. Markowitsch *et al.* suggested that the enhanced *c*-axis conductivity upon illumination might be due to the observed photoinduced contraction of the *c*-axis, which can lead to stronger interplanar coupling [71–73].

### 3.1.4. Structural Changes

Figure 4 shows the fractional change of the *c*-axis lattice parameter  $\Delta c/c$  determined from X-ray diffraction, compared to the resistivity change  $\Delta\rho/\rho$ .  $\Delta c/c$  has the same dependence as  $\rho$  and indicates a contraction of the *c*-axis, contrary to what could be expected from thermal heating [74,75]. A careful refinement of the X-ray data reveals that most of the

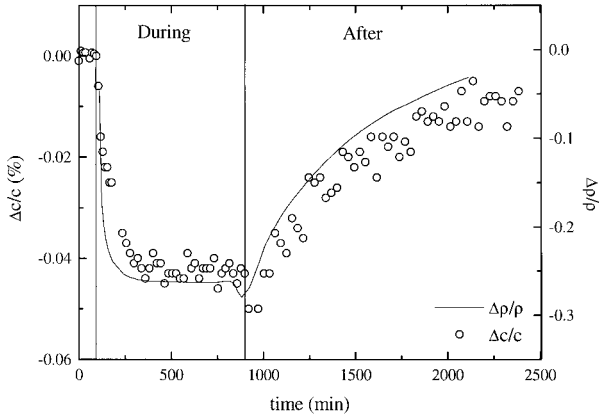


**Fig. 4.** Time dependence of the fractional change  $\Delta c/c$  of the  $c$ -axis lattice parameter and resistivity  $\Delta\rho/\rho$ . The measurements were done on a  $\text{YBa}_2\text{Cu}_3\text{O}_{6.5}$  thin film at room temperature, during and after illumination (adapted from Ref. 74).

contraction is due to a decrease of the distance between the Ba and Cu(1) in the chains [74].

Besides this clear photoinduced structural change, there is additional data, which may indicate ordering of oxygen in the CuO-chains upon illumination. Raman scattering shows an increase in intensity of several phonon lines involving vibrations of the Cu and O atoms in the CuO chains [76], as well as the photoinduced bleaching of other Raman lines associated with the CuO chains [77–80]. The time dependence of the photoinduced bleaching is comparable to the PPC and follows a stretched exponential law similar to Eq. (1) [79,80]. However, the interpretation of the Raman data is not straightforward, and several different theoretical models have been proposed that are consistent with photoinduced oxygen ordering [76–79], photoinduced oxygen *disordering* [80], or charge transfer with subsequent electron trapping [77]. It should be pointed out that while the photoinduced oxygen ordering or electron trapping are theoretical models commonly used to explain PPC (see Section 4), the photoinduced oxygen *disordering* [80] seems to be incompatible with the other observed photoinduced effects besides the bleaching of the Raman lines.

Furthermore, the bond length between the Cu(1) in the chain and the apical O(4) observed by X-ray absorption splits, into two well-defined peaks upon illumination [81], which may also indicate some local ordering. Experiments that are designed to investigate directly the effect of oxygen ordering are discussed in Section 3.1.7.

### 3.1.5. Spectral Dependence

The spectral dependence of the PPC in  $\text{RBA}_2\text{Cu}_3\text{O}_x$  investigated by many different groups [34,82–86] shows that for a given wavelength, the photoinduced magnitude in  $\text{RBA}_2\text{Cu}_3\text{O}_x$  depends only on the number of photons per surface area exciting the sample. This implies that the photoexcitation is mainly a one photon process [53]. Figure 5 shows the spectral dependence with an onset at 1.6 eV, several smaller peaks from 1.6–3.3 eV [34,82,83,85], and a very pronounced peak at 4.1 eV [34]. The peaks in the visible energy range (1.6–3.3 eV) are generally attributed to transitions in the  $\text{CuO}_2$  planes [34,82,83], while the peak at 4.1 eV is associated with a transition in the CuO chains [34]. In particular the strong peak at 4.1 eV may give some insight into the mechanism responsible for the PPC. This peak has been attributed to a  $3d_{3z^2-1}$  to  $4p_x$  electronic transition of  $\text{Cu}^{1+}$  atoms in an O-Cu-O dumbbell [87]. These  $\text{Cu}^{1+}$  atoms are located in the CuO chains and have an oxygen vacancy on both sides. The enhancement that is observed for the PPC at 4.1 eV is much stronger than what can be expected from the increased absorption at this energy alone [34]. Thus, this implies that the PPC is strongly enhanced as soon as an electron-hole pair is created in close proximity to an oxygen vacancy, which is also consistent with the observed doping dependence (see Section 3.1.6). Therefore the strong enhancement of PPC for an electronic transition located next to the oxygen vacancies supports the electron-trapping model of PPC (see Section 4).

Bud’ko *et al.* [83] found that the peak positions in

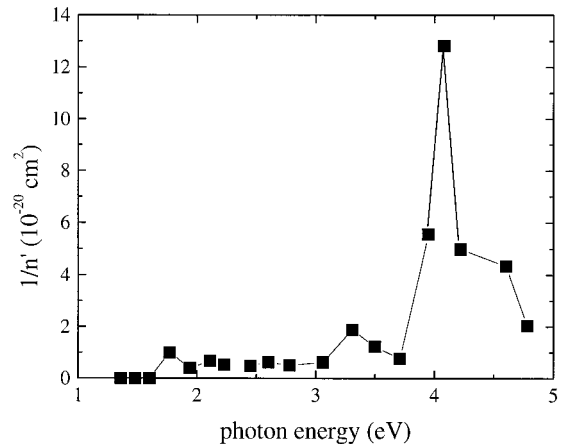


**Fig. 5.** Spectral efficiency of the persistent photoconductivity for  $\text{GdBa}_2\text{Cu}_3\text{O}_{6.3}$ .  $n'$  is the number of photons per unit area necessary for a 2% decrease in the resistance (adapted from Ref. 34).

the spectral dependence do not change with oxygen concentrations  $x$  in the range  $6.35 < x < 6.75$ . On the other hand, in very highly doped samples Markowitsch *et al.* [85] observed a finite efficiency for the persistent photoconductivity even below the 1.6 eV threshold, in contrast to the spectral dependence for  $x \leq 6.75$  [34,82–84,86]. Similar PPC was also observed in  $\text{YBa}_2\text{Cu}_3\text{O}_x$  upon irradiation with X-rays [88].

It was shown above that close to room temperature the excited state relaxes to the original one. It is also possible to quench partially the PPC in  $\text{YBa}_2\text{Cu}_3\text{O}_x$  thin films using infrared radiation (980–1480 nm) while keeping the thin film at low temperatures [89,90]. The quenching time scale is several orders of magnitude shorter than the thermal one at room temperature and the quenching is reversible by illumination with visible light. Figure 6 shows the infrared quenching after photodoping with visible light. The wavelength dependence of the infrared quenching suggests that the average trap depth of the potential well is near 1 eV, in agreement with the value determined from the activation energy of the thermal relaxation [53].

### 3.1.6. Doping Dependence

All photoinduced changes described thus far are similar to increasing the oxygen content  $x$  in the  $\text{RBA}_2\text{Cu}_3\text{O}_x$  films. Because in all the experiments the samples are either in vacuum, liquid He, N, or an inert gas, intake of oxygen by the sample can be excluded. At the same time, because the photoinduced effects are fully reversible a loss of oxygen can also be excluded. Nevertheless, it is very interesting to study the influence of oxygen stoichiometry on the persistent photoconductivity [50,58]. The normalized photoinduced conductivity change increases monotonically with decreasing oxygen content  $x$  (Fig. 7), indicating that an increased number of oxygen vacancies in the CuO chains enhances the PPC [50]. Furthermore, oxygen vacancies are necessary for the PPC, even if the doping level is decreased by different means, for instance with Pr doping in  $\text{Y}_{1-z}\text{Pr}_z\text{Ba}_2\text{Cu}_3\text{O}_x$  [74], or Sr doping in  $\text{YSr}_z\text{Ba}_{2-z}\text{Cu}_3\text{O}_x$  [91]. PPC is observed only in oxygen-deficient ( $x < 7$ ) films. Interestingly, the magnitude of the PPC and PPS in oxygen-deficient thin films increases with Pr doping and the relax-

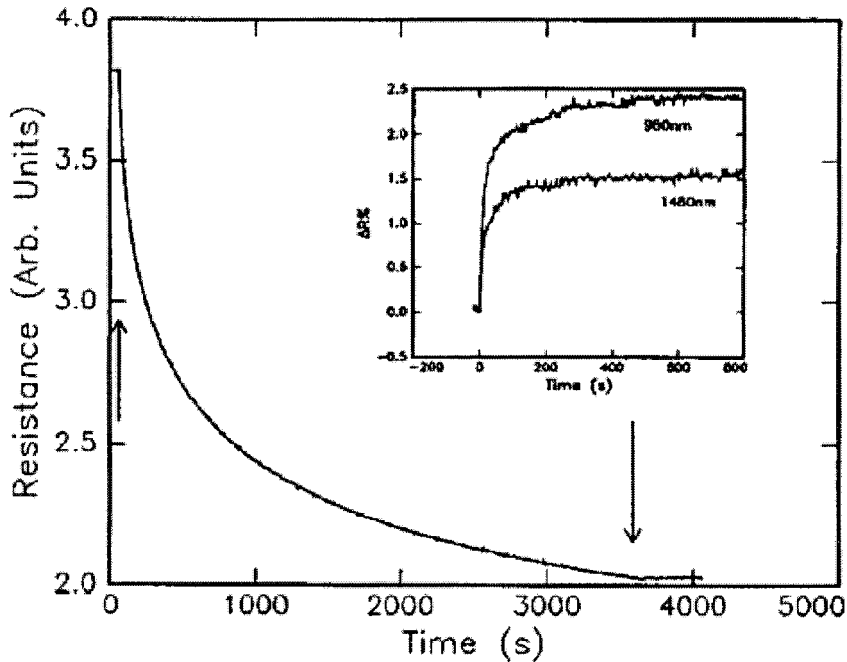


**Fig. 6.** Time-dependent resistance during argon ion laser illumination of  $\text{YBa}_2\text{Cu}_3\text{O}_{6.4}$  sample immersed in liquid nitrogen. The upward arrow indicates when the sample is exposed to visible laser light. The downward arrow indicates when the light is blocked. The inset shows time-dependent change in resistance for the same sample upon illumination with 980-nm (25-mW) and 1480-nm (56-mW) light (adapted from Ref. 89).

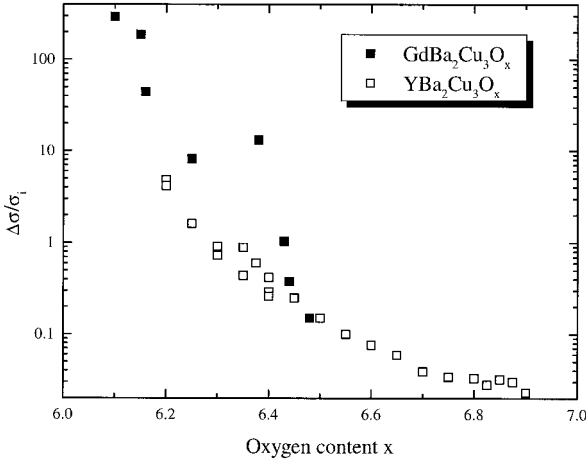


**Fig. 7.** Relative change in conductivity  $\Delta\sigma/\sigma_i$  as a function of oxygen content  $x$  of  $R\text{Ba}_2\text{Cu}_3\text{O}_x$ . ■ =  $\text{GdBa}_2\text{Cu}_3\text{O}_x$ ; □  $\text{YBa}_2\text{Cu}_3\text{O}_x$ . (Adapted from Ref. 50.)

ation time for the thermal relaxation decreases with increasing Sr content  $z$ . Unfortunately it is not clear whether the Pr or Sr doping modifies the energy barrier for the relaxation. Recently it was shown by Lin *et al.* [92] that PPC in  $R\text{Ba}_2\text{Cu}_3\text{O}_x$  is not only limited to underdoped samples, but can also be observed in overdoped  $\text{Y}_{0.5}\text{Ca}_{0.5}\text{Ba}_2\text{Cu}_3\text{O}_x$  provided that the sample is oxygen deficient. In this case, there is a decrease of  $T_c$  with illumination, while the conductivity still increases as observed also in the overdoped  $\text{Tl}_2\text{Ba}_2\text{CuO}_{6+\delta}$  compounds [93]. Thus, persistent photoconductivity can unambiguously determine the doping state of a high  $T_c$  superconductor.

### 3.1.7. Persistent Photoconductivity vs. Oxygen Ordering

The experimental results presented so far are very similar to resistivity and structural changes observed during room temperature annealing of oxygen deficient  $R\text{Ba}_2\text{Cu}_3\text{O}_x$  samples rapidly quenched from higher temperatures [94,95]. Several groups explained the effect of room temperature annealing by ordering of oxygen in the CuO chain layers [94–96]. In addition, a few experiments point toward an increased order of oxygen in the CuO chains with illumination [76,81], which motivated Osquiguil *et al.* [97] to suggest oxygen ordering as the underlying mechanism for the PPC. Therefore, it is interesting to investigate further the relationship between PPC and oxygen order in the CuO chains.

Müller *et al.* [98] showed that in rapidly quenched oxygen deficient  $\text{YBa}_2\text{Cu}_3\text{O}_x$  the magnitude of the PPC correlates with the progress of the room temperature annealing. On the other hand, Guimpel *et al.* [99] showed that PPC and oxygen disorder are independent from each other, although the relaxation dynamics for both cases is the same and may therefore involve the movement of oxygen in the chains. Furthermore, photoluminescence measurements by Federici *et al.* [90,100] suggest that the PPC is due to trapped electrons (e.g., in the oxygen vacancies in the CuO chains), thus oxygen ordering might not be important for these effects. Nevertheless, positron lifetime measurements showed that illumination leads to a change of the local electron density in the charge reservoir layer [101].

## 3.2. Other High $T_c$ Superconductors

### 3.2.1. $\text{Tl}_2\text{Ba}_2\text{CuO}_{6+\delta}$

As discussed, oxygen vacancies in the CuO chains play an important role for the PPC in  $R\text{Ba}_2\text{Cu}_3\text{O}_x$ . Therefore, it is interesting to investigate other high  $T_c$  superconductors without CuO chains such as  $\text{Tl}_2\text{Ba}_2\text{CuO}_{6+\delta}$ .  $\text{Tl}_2\text{Ba}_2\text{CuO}_{6+\delta}$  has one CuO<sub>2</sub> plane per unit cell and its  $T_c$  is easily varied between 0–90 K by oxygen doping. As shown in Fig. 8, this material also exhibits PPC [93], thus proving that CuO chains are not a necessary structural ingredient for this effect. Illumination of  $\text{Tl}_2\text{Ba}_2\text{CuO}_{6+\delta}$  with visible light leads to a decrease in  $T_c$  and a decrease in  $\rho$ , thus giving an unambiguous evidence for the overdoped nature of the sample.

There are further differences between the PPC in  $R\text{Ba}_2\text{Cu}_3\text{O}_x$  and  $\text{Tl}_2\text{Ba}_2\text{CuO}_{6+\delta}$ . The excitation and relaxation times are much shorter in  $\text{Tl}_2\text{Ba}_2\text{CuO}_{6+\delta}$ , and even at low temperatures ( $\approx 30$  K), there is a measurable thermal relaxation. The excitation and relaxation times follow again a stretched exponential law [see Eq. (1)]. Contrary to  $R\text{Ba}_2\text{Cu}_3\text{O}_x$ , PPC in  $\text{Tl}_2\text{Ba}_2\text{CuO}_{6+\delta}$  can be quenched fully with infrared light, and its sign can change even as a function of illumination wavelength and doping level [93]. The spectral dependence (Fig. 9) shows a clear threshold at 1.4 eV, similar to the PPC onset observed in  $R\text{Ba}_2\text{Cu}_3\text{O}_x$  and the charge transfer gap observed in insulating cuprates [102]. This is surprising, because  $\text{Tl}_2\text{Ba}_2\text{CuO}_{6+\delta}$  is overdoped and therefore clearly in the metallic state. Besides the PPC in  $\text{Tl}_2\text{Ba}_2\text{CuO}_{6+\delta}$ , it has also been shown that  $\text{Tl}_2\text{Ba}_2\text{CaCu}_2\text{O}_8$  exhibits metasta-

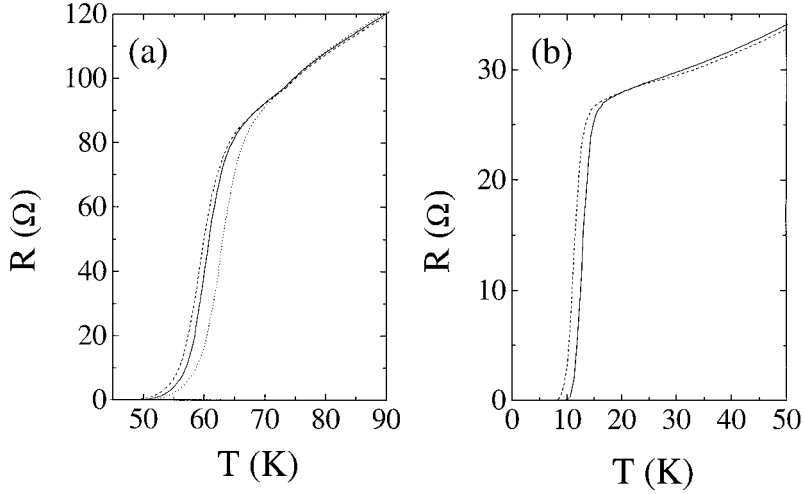


**Fig. 8.** Resistance vs. temperature during (dashed or dotted line) and without (solid line) illumination for  $\text{Tl}_2\text{Ba}_2\text{CuO}_{6+\delta}$  thin films with different doping. (a) Initial  $R(T)$  (solid line) with  $T_c = 60$  K and  $R(T)$  during illumination with 1000-nm (dotted line) and 400-nm (dashed line) light. (b) Initial  $R(T)$  with  $T_c = 13$  K (solid line) and  $R(T)$  during illumination with 440-nm (dashed line) light (adapted from Ref. 93).

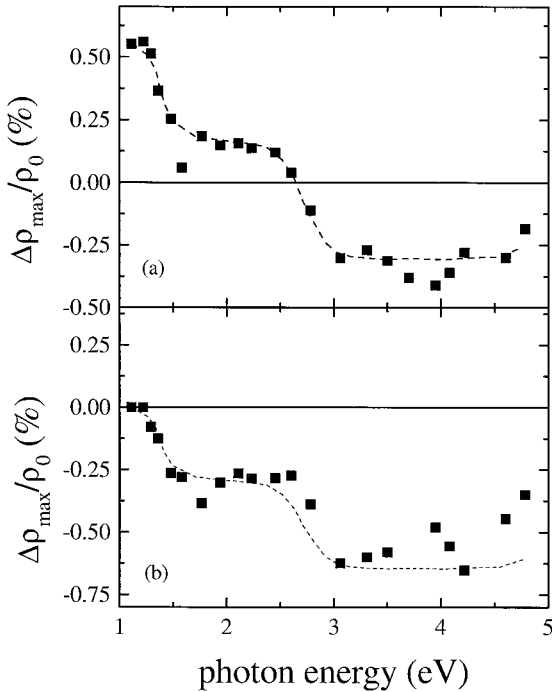


**Fig. 9.** Spectral dependence of persistent photoconductivity in  $\text{Tl}_2\text{Ba}_2\text{CuO}_{6+\delta}$  for the  $T_c = 60$  K (a) and the  $T_c = 13$  K (b) sample. The dashed lines are guides to the eye (adapted from Ref. 93).

ble photoinduced changes of its magnetic properties [103].

### 3.2.2. $\text{Bi}_2\text{Sr}_2\text{CaCu}_2\text{O}_{8+\delta}$

Initially, long-time illumination on  $\text{Bi}_2\text{Sr}_2\text{CaCu}_2\text{O}_{8+\delta}$  thin films were performed by Maenhout [104] in the overdoped and in the underdoped state. The films were illuminated at 100 K during 8 hours with green laser light ( $\lambda = 514.5$  nm) (total photon dose of  $3 \times 10^{23}$  photons/cm<sup>2</sup>). No PPC or PPS was found in these experiments. On the other hand, Tanabe *et al.* [105] showed that illumination of  $\text{Bi}_2\text{Sr}_2\text{CaCu}_2\text{O}_{8+\delta}$  can lead to a *permanent* irreversible photoinduced *increase* of the resistivity. Moreover, this permanent PPC is very similar to the time-dependent resistivity change observed for  $\text{Bi}_2\text{Sr}_2\text{CaCu}_2\text{O}_{8+\delta}$  thin film kept at 50°C [93], implying that this is most likely due to oxygen loss in these films and thus unrelated to the *reversible* PPC observed in other high  $T_c$  superconductors.

Recently a reversible change of conductivity with illumination was found in  $\text{Bi}_2\text{Sr}_2\text{Ca}_{1-x}\text{Y}_x\text{Cu}_2\text{O}_{8+\delta}$  [106,107]. This sample is insulating and shows a decrease of resistivity upon illumination, which even at low temperatures slowly relaxes thermally back to its initial value (Fig. 10). This is remarkably different

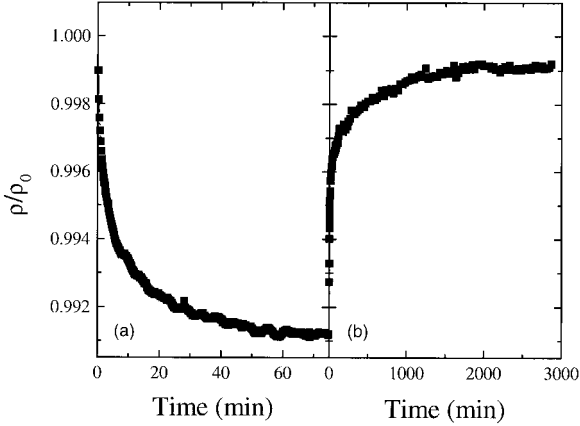


**Fig. 10.** Time dependence of persistent photoconductivity in  $\text{Bi}_2\text{Sr}_2\text{Ca}_{1-x}\text{Y}_x\text{CuO}_{8+\delta}$  during (a) excitation and (b) relaxation (adapted from Ref. 106).

from the photoinduced effects in pure  $\text{Bi}_2\text{Sr}_2\text{CaCu}_2\text{O}_{8+\delta}$ .

### 3.2.3. Other Cuprates

The results on  $\text{Tl}_2\text{Ba}_2\text{CuO}_{6+\delta}$  and  $\text{Bi}_2\text{Sr}_2\text{Ca}_{1-x}\text{Y}_x\text{Cu}_2\text{O}_{8+\delta}$  suggest that persistent photoconductivity might be a general feature of high  $T_c$  superconductors. Illumination of  $\text{La}_{2-y}\text{Sr}_y\text{CuO}_4$  thin films has been made for different doping concentration  $y$  for which

$\text{La}_{2-y}\text{Sr}_y\text{CuO}_4$  is insulating, metallic or superconducting. Maenhoudt [104] observed no difference between the resistivity before and after illumination and no change in  $T_c$  for all Sr concentrations in  $\text{La}_{2-y}\text{Sr}_y\text{CuO}_4$ . On the other hand, as shown in Fig. 11, preliminary data on other  $\text{La}_{2-y}\text{Sr}_y\text{CuO}_4$  films by Hoffmann *et al.* [108] suggest that there is persistent photoconductivity, even in this system. The non-monotonic slope of the normal state resistivity of the sample in Fig. 11 suggests that this particular sample consists of at least two different phases, one that dominates the conductivity at low temperatures, while the other one is more important at high temperatures. Using this assumption would imply that only the phase that dominates the conductivity at high temperatures shows PPC [108]. However, the nature of this phase remains unclear at this time. It is possible that the  $\text{La}_{2-y}\text{Sr}_y\text{CuO}_4$  phase showing PPC is oxygen deficient, which could explain the discrepancy to the earlier results. Clearly, this point needs more investigation. Other interesting systems are the “electron” doped cuprates, but so far no persistent photoinduced phenomena have been reported in  $\text{Nd}_{2-x}\text{Ce}_x\text{CuO}_4$  [42].

## 4. THEORETICAL MODELS OF PHOTODOPING

Several models have been proposed to explain photodoping experiments in HTSC thin films. Kudi-

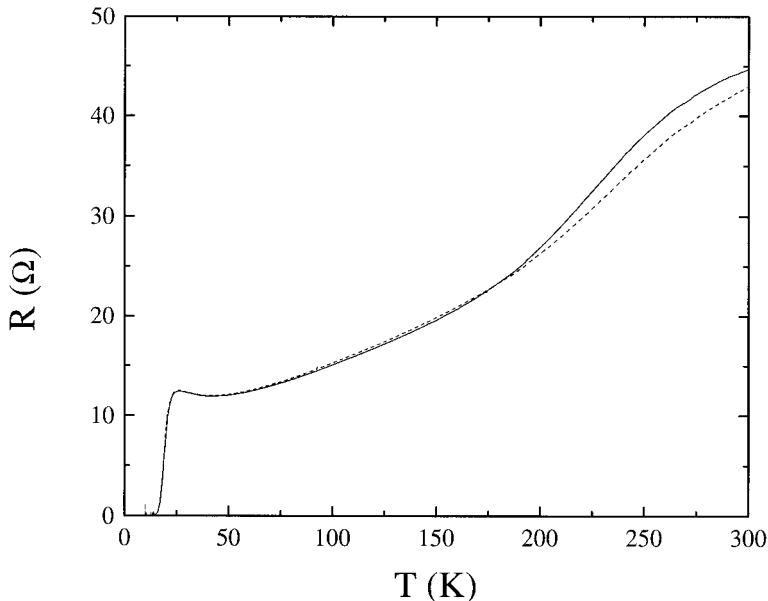


**Fig. 11.** Temperature dependence of the resistivity of a  $\text{La}_{2-y}\text{Sr}_y\text{CuO}_4$  thin film before (solid line) and after (dashed line) illumination (adapted from Ref. 108).

nov *et al.* [53] suggest that illumination causes photoexcitation of electron-hole pairs with the subsequent trapping of electrons by defects. For  $\text{YBa}_2\text{Cu}_3\text{O}_x$  these defects are oxygen vacancies in the  $\text{CuO}$  chains where normally an oxygen ion would be located in a fully oxygenated sample. This capture process creates excess mobile holes transferred into extended states in the  $\text{CuO}_2$  planes with the consequent enhancement of the transport properties [109]. Krylov [110] suggested that the electron trapping at the oxygen vacancies is due to a local structural change, which gives rise to an energy barrier. This can also explain the observed photoinduced structural changes (see Section 3.1.4.). Numerical estimates of the barrier height and the relaxation time agree well with the experimental data [110]. Electron trapping is more pronounced for oxygen-deficient films owing to the larger concentration of oxygen vacancies where electrons can be trapped [50]. The electron trapping mechanism is also supported by the observed spectral dependence [34].

A variation of this defect-trapping model was suggested by Kudinov [111]. In this model, the electrons are actually trapped in the  $\text{CuO}$  chain fragments instead of at the oxygen vacancies. This suggests that PPC should vanish at low doping, contrary to experimental observations (see Section 3.1.6.).

The PPC and PPS in  $\text{RBa}_2\text{Cu}_3\text{O}_x$  seem to be strikingly similar to sample doping with oxygen. Osquiguil *et al.* [97] proposed that photons assist the diffusion of oxygen by inducing local electric fields in the chains, which in turn increases chain length, thereby enhancing the doping and consequently the PPC and PPS. It seems that photoinduced oxygen ordering should peak at  $x = 6.5$  where maximal oxygen disorder exists [50]. It should be noted that there is an important difference between oxygen ordering in quenched samples and the photoinduced effects. While in the quenched samples the oxygen in the  $\text{CuO}$  chains order during room temperature annealing, the oxygen has to disorder from a metastable state in the photoexcited samples during room temperature relaxation. Also, it has been shown that the photoexcitation process is indeed independent from oxygen disorder induced by quenching [99]. Thus the validity of the oxygen-ordering model seems questionable.

All the models described so far rely in one way or another on the  $\text{CuO}$  chains, which are specific to  $\text{RBa}_2\text{Cu}_3\text{O}_x$ . But the recent results on  $\text{Tl}_2\text{Ba}_2\text{CuO}_{6+\delta}$  and  $\text{Bi}_2\text{Sr}_2\text{Ca}_{1-x}\text{Y}_x\text{Cu}_2\text{O}_{8+\delta}$  show that the  $\text{CuO}$  chains are not essential for persistent photoconductivity.

The electron-trapping model using oxygen vacancies as traps for photoexcited electrons can easily be extended to these types of materials. In this case localized states in the charge reservoirs, spatially separated from the  $\text{CuO}_2$  planes, are required to act as electron traps. In  $\text{Tl}_2\text{Ba}_2\text{CuO}_{6+\delta}$  there are two well-known types of structural defects which might trap the photogenerated electrons [112]: Cu substituted for Tl in the TlO layers, and interstitial oxygen between the TlO layers. For  $\text{Bi}_2\text{Sr}_2\text{Ca}_{1-x}\text{Pr}_x\text{Cu}_2\text{O}_8$  it has been suggested that there are localized states, even for superconducting samples [113].

To explain the absence of PPC and PPS in  $\text{Bi}_2\text{Sr}_2\text{CaCu}_2\text{O}_8$ , Maenhoudt [104] suggests that the energy levels of oxygen vacancies are situated deeper in the valence band and therefore cannot trap photocreated electrons. As a consequence the electrons and holes recombination is very fast.

## 5. ILLUMINATION OF $\text{YBa}_2\text{Cu}_3\text{O}_x$ JOSEPHSON JUNCTIONS

### 5.1 Introduction

A GBJJ is made of a weak link, the grain boundary (GB), between two fully oxygenated banks of  $\text{YBa}_2\text{Cu}_3\text{O}_7$ . This GB is presumably an oxygen-deficient region. Thus, illuminating the whole junction will induce photodoping only in the oxygen-deficient GB region, without affecting the generally fully oxygenated banks. It was originally suggested by Kudinov *et al.* [53] that this can be used to tune in situ these weak links.

The effect of photodoping on the conductivity can be easily investigated by measuring the transport properties of HTSC thin films in the normal state before and after illumination. However, instead of measuring the critical temperature, which is given by zero electrical resistance, it is easier to measure the PPS on a GBJJ than on HTSC thin films, because it is easier to measure the PPS of a weaker superconductor than of a strong superconductor where other phenomena like flux flow can take place. Moreover, the change, by photodoping, of the superconducting and normal transport properties of the oxygen barrier of GBJJ can be detected in the  $I(V)$  curves for the same temperature, depending on the voltage range considered: An enhancement of the critical current is measured at zero voltage whereas the increase of the conductivity is measured at high voltages.

## 5.2. GBJJs

### 5.2.1. DC Josephson Properties

The first investigation of the effect of photoinduced hole doping on GBJJs as well as step edge junctions has been made by Tanabe *et al.* [21] in 1994. In these experiments, GBJJ were illuminated with visible light using He-Ne laser coupled to a multimode optical fiber with a core of  $50\ \mu\text{m}$ . In this experiment the power density is approximately  $100\ \text{W}/\text{cm}^2$ , which is very high. However, the illumination-induced temperature rise was estimated to be less than  $0.5\ \text{K}$  and therefore the sample heating is not expected to have any substantial influence. Figure 12 shows typical  $I(V)$  characteristics for three different time illumination up to 1000 minutes for a  $10\text{-}\mu\text{m}$  wide bicrystal junction illuminated at  $40\ \text{K}$ . There is an increase of the critical current  $I_c$  of approximately 20–40% and a decrease of the normal state resistance  $R_n$ , such that the  $I_c R_n$  product increases with illumination. This behavior of photoinduced hole doping of  $\text{YBa}_2\text{Cu}_3\text{O}_x$  GB junction indicates that the GB is a low oxygenated barrier [114]. Hoffmann *et al.* [115] and Elly *et al.* [22] showed a similar enhancement of the critical current  $I_c$  and a decrease of the normal state resistance of GBJJ. They have shown that the critical current  $I_c$  is modulated by an applied magnetic field, which is in good agreement with the theoretical curve  $I_c = I_{c,0} |\sin(\pi\phi)/(\pi\phi)|$  where  $\phi$  is the normalized flux  $\phi = \Phi/\Phi_0$  flowing perpendicularly through the junction barrier, in units of flux quantum  $\Phi_0 = h/2e$ . Figure 13 shows the magnetic field dependence of the critical current before and

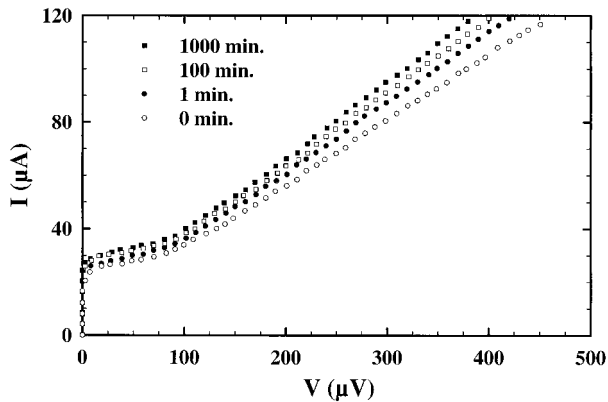


**Fig. 12.** Time dependence of the  $I(V)$  characteristics of a GBJJ at  $40\ \text{K}$  before and after 1, 100, and 1000 min illumination (adapted from Ref. 21).

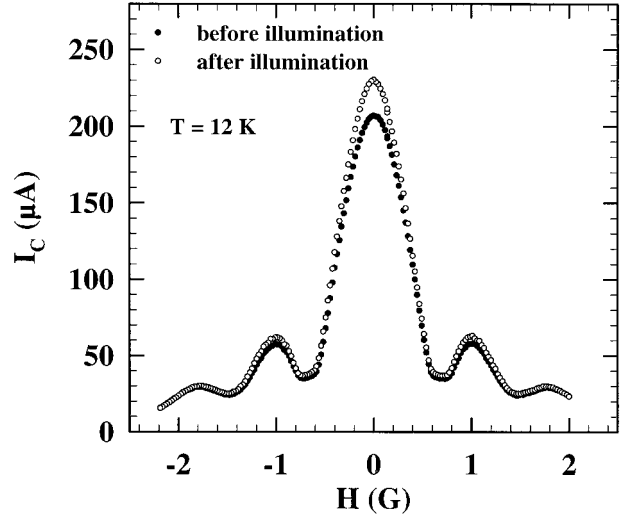


**Fig. 13.** Magnetic field dependence of the critical current before and after illumination (adapted from Ref. 22).

after illumination. The curves before and after illumination are typical for a GBJJ without substantial changes in their shape indicating that the Josephson effect is maintained after illumination although with an enhanced intensity. The highest  $I_c$  enhancement is obtained for zero magnetic field while the magnetic field periodicity does not change by photodoping. This implies that the magnetic field penetration depth  $\lambda_{ab}$ , which governs this periodicity, does not change by photodoping. This can be easily understood, because the banks on either side of the GBJJ are fully oxygenated and thus not affected by illumination and the penetration depth is large compared to the width of the grain boundary, i.e., the oxygen-depleted region.

From measurements of the Fraunhofer pattern it is possible to determine the magnetic fields at which the critical current has minima or maxima and then obtain information on the  $ab$ -plane penetration depth  $\lambda_{ab}$ . The precise determination of that magnetic fields for different temperatures enables to determine the temperature dependence of  $\lambda_{ab}(T)$  which can give information on the symmetry of the superconducting gap. This temperature dependence of  $\lambda_{ab}$  is consistent with the energy gap having either anisotropic  $s$ -wave or  $d$ -wave symmetry (or mixture of  $s$ - and  $d$ -wave) [116,117]. Because illumination of the GBJJ affects the oxygen deficient barrier without changing  $\lambda_{ab}(T)$ , the symmetry of the superconducting gap, a property related to the banks of the GBJJ, does not change.

As described in this section, most experiments on photoinduced effects in GBJJs were done using  $\text{YBa}_2\text{Cu}_3\text{O}_x$  GBJJ. Additionally, Osoria and Prieto [118] showed recently that reversible photoinduced effects can also be observed in  $\text{Bi}_2\text{Sr}_2\text{CaCu}_2\text{O}_{8+\delta}$  GBJJs. In these junctions the normal state resistance is unchanged with illumination while the critical current increases from  $30 \mu\text{A}$  to  $220 \mu\text{A}$  (corresponding to  $I_c R_n = 54 \mu\text{V}$  before and  $I_c R_n = 400 \mu\text{V}$  after illumination). This observation of reversible photoinduced effects in  $\text{Bi}_2\text{Sr}_2\text{CaCu}_2\text{O}_{8+\delta}$  GBJJs is particularly intriguing, because so far in  $\text{Bi}_2\text{Sr}_2\text{CaCu}_2\text{O}_{8+\delta}$  thin films without cation substitution there have not been any reversible photoinduced effects observed (see Section 3.2.2). Recent experiments by Gilabert *et al.* [119] on  $\text{Bi}_2\text{Sr}_2\text{CaCu}_2\text{O}_{8+\delta}$  grain boundary tunnel junctions also indicate that PPC and PPS effects exist in these junctions.

### 5.2.2. Normal State Resistance and $I_c R_n$ Product

Figure 14 shows the time dependence of the normal state resistance of GBJJ. For convenience a point of bias current polarization in the  $I(V)$  curve (for example  $0.5 \text{ mA}$ ) is used and the voltage is measured as a function of illumination time. The resistance has a sharp decrease at the beginning of the illumination and saturates after a few hours. This behavior is analogous to the PPC effect found in  $\text{YBa}_2\text{Cu}_3\text{O}_x$  thin films. The maximum relative decrease of the resistivity is of the order of 5% for a GBJJ with  $T_c \approx 90 \text{ K}$  but this can be more for GBJJs with lower  $T_c$  ( $\approx 60 \text{ K}$ ) [120]. Similarly to thin films, the time dependence can be fitted to

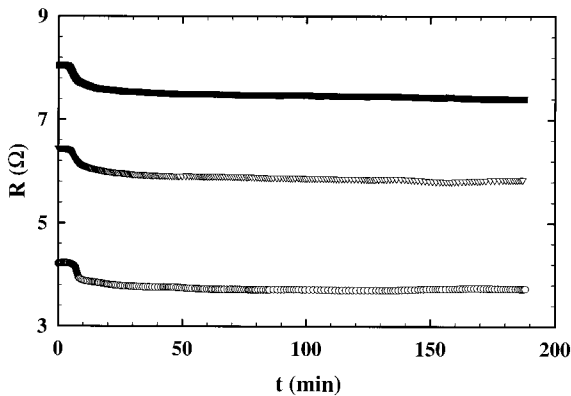


**Fig. 14.** Time dependence of the resistance of a GBJJ for three bias currents: 50, 200, and  $500 \mu\text{A}$  (adapted from Ref. 115).

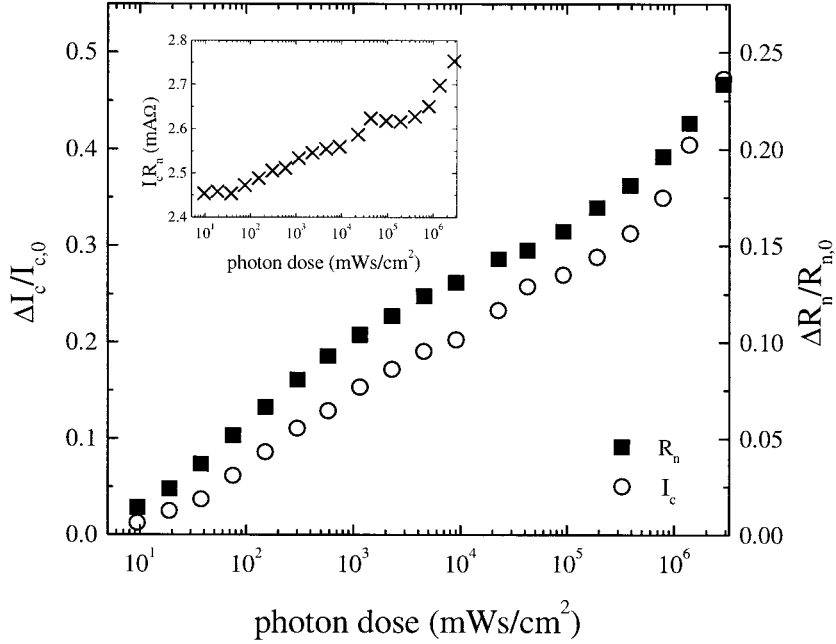
a stretched exponential [see Eq. (1)]. For the GBJJ,  $\beta$  is found to be  $\approx 0.34$  and  $n_c^{-1} \approx 10^{-19}$  to  $10^{-18} \text{ cm}^{-2}$ .

We can compare the PPC of illuminated  $\text{YBa}_2\text{Cu}_3\text{O}_x$  GBJJs with the PPC of low oxygenated thin films for different oxygen concentration  $x$  [33,115]. From this comparison we can deduce an average oxygen concentration  $x$  of the  $\text{YBa}_2\text{Cu}_3\text{O}_x$  GB. Figure 7 shows the maximum relative change of the conductivity of  $\text{YBa}_2\text{Cu}_3\text{O}_x$  oxygen-deficient thin films in a logarithmic scale as a function of the oxygen content  $x$ . Putting the maximum relative change obtained for the GBJJ we can deduce an average value  $x \approx 6.6$  for the oxygen content of the barrier of the  $T_c \approx 90 \text{ K}$  GBJJ [33, 115]. The same order of oxygen deficiency is obtained from the same analysis of the results of the  $\text{YBa}_2\text{Cu}_3\text{O}_x$  GBJJ of Tanabe *et al.* [114] realized on  $\text{SrTiO}_3$  bicrystals. For the GBJJ with lower  $T_c$  ( $T_c \approx 60 \text{ K}$ ), we find  $x \approx 6.5$  [120]. However, this is an average concentration through the barrier. The oxygen concentration decreases from  $x = 7$  in the banks down to values lower than 6.6 in the grain boundary. Thus the GBJJ is a rather complicated weak link, which can be modeled as a superconductor–semiconductor–superconductor (S-Sc-S) junction, or even a more complex structure like S-N-Sc-N-S junction where N is a normal metal [121]. The temperature dependence of the critical current in such structures has been shown to reflect such complicated structure [31,32].

Tanabe *et al.* [114] and Hoffmann *et al.* [115] have found that the increase of  $I_c$  is larger than the decrease of  $R_n$  as shown in Fig. 15 where the increase  $\Delta I_c/I_c$  and the decreases of  $\Delta R_n/R_n$  is plotted versus the photon dose. Also the increase of  $I_c R_n$  is shown in the inset. For example, after 15 min of illumination at  $12 \text{ K}$  and for zero magnetic field, the relative increase of the critical current is 11% while the relative decrease of the normal state resistance  $R_n$  is 1.5%. The increase of the critical current is thus higher than the decrease of the resistance so that the  $I_c R_n$  product after illumination has increased by 9% indicating an improvement of the superconducting properties of the weak link. These results confirm the results obtained by Tanabe *et al.* [114] and we can conclude that the weak link of GBJJ is an oxygen-deficient region.

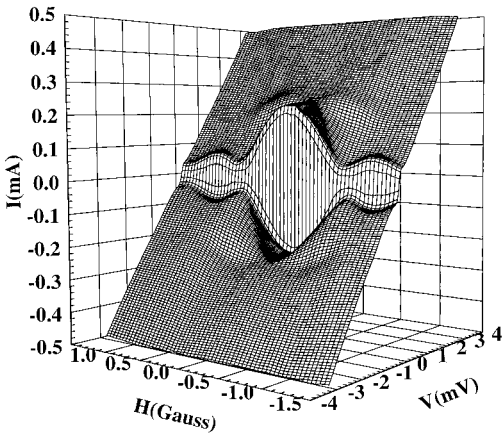
### 5.2.3. AC Josephson Properties

Figure 16 shows current-voltage  $I(V)$  characteristics at  $T = 12 \text{ K}$  for different applied magnetic fields



**Fig. 15.** Increase of the critical current  $\Delta I_c/I_c$ , decrease of the normal state resistance  $\Delta R_n/R_n$  and increase of the  $I_c R_n$  product of a GBJJ (adapted from Ref. 115).

in a three dimensional representation. The Fraunhofer pattern  $I_c(H)$  [shown in Fig. 17(a)] can be seen in the plane  $V = 0$ . Figure 16 shows also that not only the critical current  $I_c$  at zero voltage is magnetic field dependent but also structures which appear as bumps at some finite voltage and can be analyzed as Fiske resonances [122]. Due to high damping in these GBJJ, the structures appear as bumps and not as sharp Fiske steps as usually found in Josephson



**Fig. 16.** Current voltage characteristics at 12 K of a  $\text{YBa}_2\text{Cu}_3\text{O}_x$  GBJJ for different applied magnetic fields (adapted from Ref. 22).

junctions made with classical superconductors. Four such bumps are clearly seen in Fig. 16 at a voltage position depending on the length  $W$  of the GBJJ. The amplitude of these Fiske modes is magnetic field dependent.

The Fiske steps can be understood in the following way. A Josephson junction can be considered as a transmission line for electromagnetic waves. The electric field is essentially confined within the barrier region of thickness  $t$ . On the other hand, the magnetic field fills a larger region of thickness  $d = 2\lambda_L + t$  where  $\lambda_L$  is the London penetration depth in the superconducting region. For such a transmission line the phase velocity called Swihart velocity  $c$ , of an electromagnetic wave is given by  $c = c_0 (t/\epsilon d)^{1/2}$ , where  $c_0$  is the light velocity in vacuum and  $\epsilon$ ; the relative dielectric constant of the barrier. Because the region filled by the magnetic field ( $d$ ) is larger than the region filled by the electric field ( $t$ ), the velocity  $c$  is smaller than  $c_0$ . In an external magnetic field  $H$ , there may be a set of current singularities called Fiske resonances in the  $I(V)$  characteristics at voltages [123]:

$$V_n = n \frac{h}{2e} \frac{c}{2W} = n \Phi_0 \frac{c}{2W}. \quad (4)$$

These geometrical resonances occur when the length

$W$  of the junction corresponds just to an integer number  $n$  of half wavelengths of the Josephson current density wave  $j = j_c \sin(\omega t - ky)$  running in the  $y$  direction along the junction.

The amplitude  $\Delta I(\phi)$  of these resonances as a function of the normalized magnetic flux  $\phi = \Phi/\Phi_0$  through the junction is given theoretically by [123]:

$$\Delta I(\phi) = I_c \left( \frac{Q}{4\pi^2} \right) \left( \frac{W}{\lambda_J} \right)^2 F_1^2(\phi), \quad (5)$$

with

$$F_1^2(\phi) = \left[ \frac{2\phi}{\left(\phi + \frac{1}{2}\right)} \right]^2 \left[ \frac{\sin\left(\pi\phi - \frac{\pi}{2}\right)}{\pi\phi - \frac{\pi}{2}} \right]^2, \quad (6)$$

where  $\lambda_J = [\Phi_0/(2\pi\mu_0 dj_c)]^{1/2}$  is the Josephson penetration length,  $j_c$  the critical current density and  $Q$  the quality factor. This theoretical function  $F_1^2$  is plotted in Fig. 17(b) for a typical GBJJ. The experimental results are in a qualitative agreement with this  $F_1^2(\phi)$

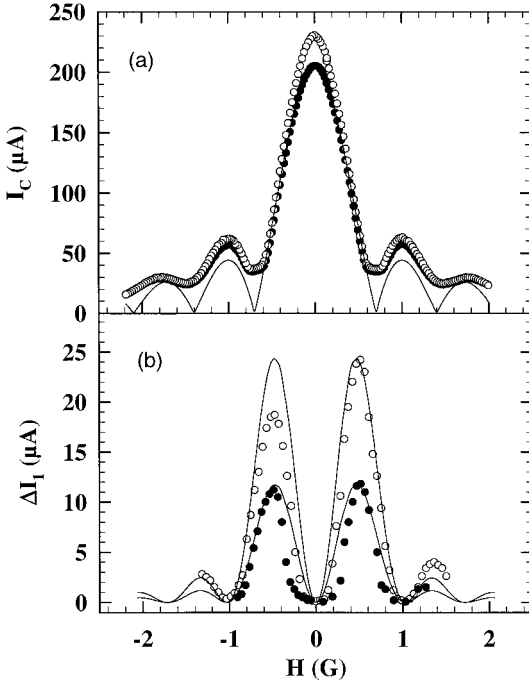


**Fig. 17.** (a) Critical current versus magnetic field (Fraunhofer pattern) before (●) and after illumination (○) and theoretical curve  $|\sin(\pi\phi)/(\pi\phi)|$ . (b) Amplitude of the Fiske resonance (first mode) versus magnetic field before (●) and after illumination (○). The solid line is the theoretical curve  $F_1^2$  given by Eq. (6) (adapted from Ref. 22).

curve. Comparing the magnetic field periodicity of the Fiske step with the magnetic field periodicity of the Fraunhofer pattern shown in Fig. 17(a), we find that the maxima and minima found experimentally are in agreement with the theoretical values: The first maximum of the amplitude of the Fiske step is at  $0.7\Phi_0$ , the second maximum is at  $1.5\Phi_0$ , and the first minimum is at  $\Phi_0$  [124,125].

The effect of 30-min illumination on the  $I(V)$  curves is shown in Fig. 18 at  $T = 12$  K for  $H = 0$  G (a) and  $H = 0.56$  G (b) corresponding to the maximum amplitude of the Fiske bump for the GBJJ used. These curves have been recorded when the light is switched off, so that there is no correction due to heating effects. For example, at  $H = 0.56$  G, the position of the Fiske resonance shifts from 0.8 mV up to a maximum position  $V_1 = 1.15$  mV for cumulative illumination time. This is a 44% change. In Fig. 19, we can see the amplitude of the Fiske step increasing by a factor of about 2 and the position moving up to a maximum voltage position, which does not move even after continuing the illumination. Again, the  $I(V)$  curves have been recorded without illumination after different cumulative times of illumination. As

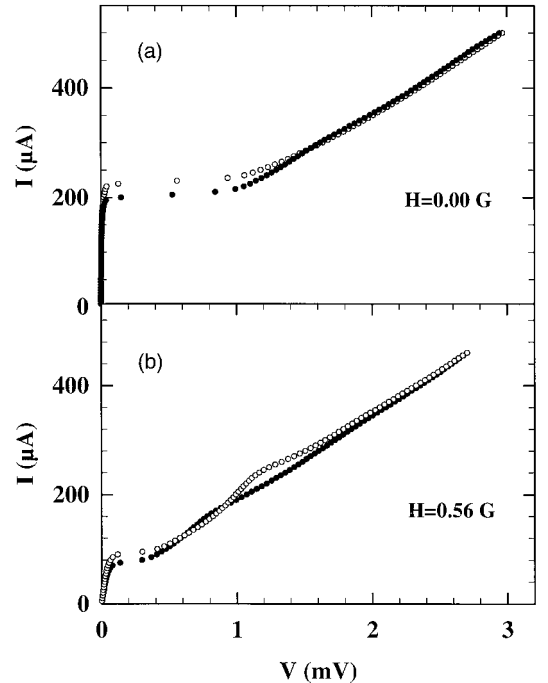


**Fig. 18.** (a)  $I(V)$  curves at  $T = 12$  K,  $H = 0$  G before (●) and after illumination (○). (b)  $I(V)$  curves at  $T = 12$  K,  $H = 0.56$  G corresponding to the maximum amplitude of the Fiske bump before (●) and after illumination (○) (adapted from Ref. 116).

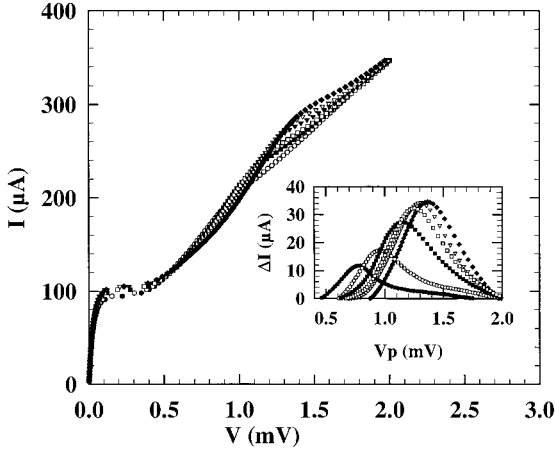


**Fig. 19.**  $I(V)$  curves at  $T = 12$  K,  $H = 0.56$  G before and after 0.5, 3, 5, 7, 11, and 20 min illumination time (adapted from Ref. 126).

with the thin films, the excitation time scales inversely with the intensity. This means that again the total photon dose is the relevant parameter.

In Fig. 17 (b) we see the magnetic field dependence of the maximum amplitude of the Fiske reso-

nance before and after illumination. The qualitative magnetic field dependence remains unchanged with illumination. The Fiske resonance amplitude increases with illumination; however, the magnetic field positions of the minima remain almost unchanged. This implies that the order  $n$  of the Fiske step is unchanged after illumination. Thus we can study the voltage position of the Fiske resonance versus the mode number  $n$ . The amplitude decreases for increasing mode number  $n$  and thus it is hard to see the modes higher than  $n = 1$ . However, if we subtract the 3D  $I(V)$  curves before and after illumination as shown Fig. 20, then we can see clearly the first three modes. Figure 21 shows the dependence of the voltage positions  $V_n$  as a function of the mode number  $n$  before and after illumination. From the linear slope, and using Eq. (4), we find for the value of the Swihart velocity  $c = 3.9 \times 10^6$  m/s before illumination and  $c = 5.5 \times 10^6$  m/s after illumination [22,126].

We have studied the maximum voltage position  $V_1$  corresponding to the first mode of the Fiske resonances for GBJJ of different length  $W$  before and after illumination. Figure 22 shows the linear variation of these voltage positions  $V_1$  as a function of

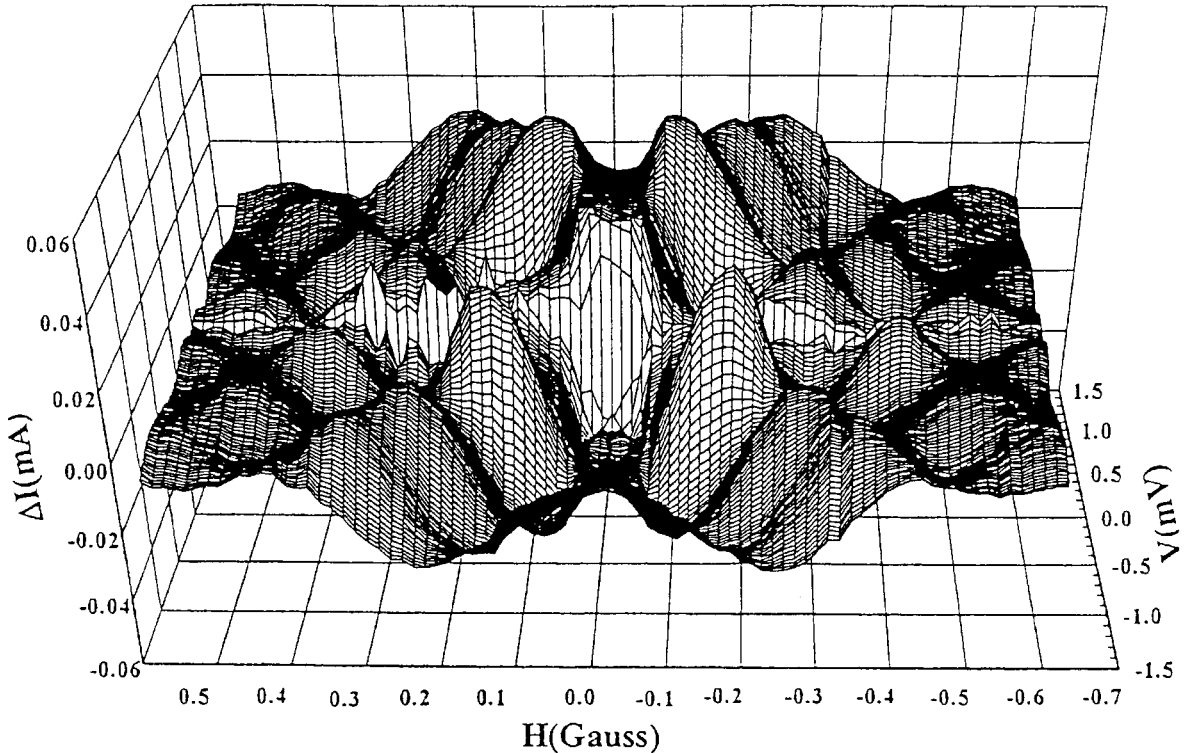


**Fig. 20.** Difference between the  $I(V)$  curves before and the  $I(V)$  curves after illumination for different applied magnetic field (adapted from Ref. 126).

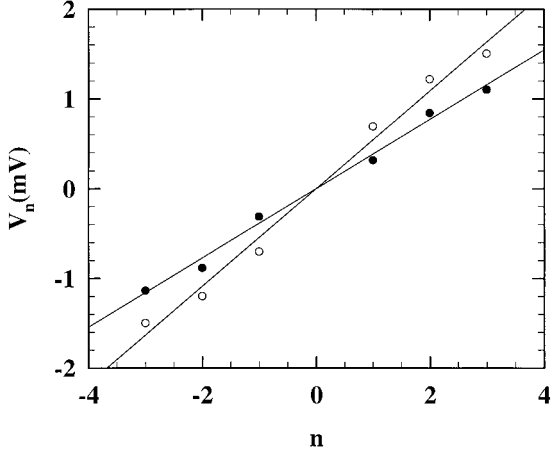


**Fig. 21.** Dependence of the voltage position  $V_n$  as a function of the mode number  $n$  before (●) and after illumination (○) (adapted from Ref. 126).

$1/W$  as expected from Eq. (4). From the linear slope we can determine the Swihart velocity and find  $c = 4 \times 10^6$  m/s before illumination, in good agreement with the value obtained from the higher-order Fiske modes. This linear dependence means also that the GBJJ made on the same bicrystal have homogeneous barriers with the same relative dielectric constant and same thickness  $t$ . These maximum voltage positions  $V_1$  show also after illumination a linear variation versus  $1/W$ . From the slope we can deduce a value  $c = 5.6 \times 10^6$  m/s for the Swihart velocity after illumination, again in good agreement with the value obtained from the higher-order Fiske modes. After illumination (noted with the index  $L$ ) the current bump is

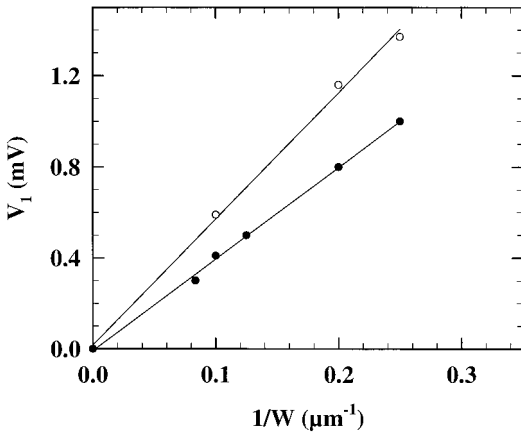


**Fig. 22.** Voltage position  $V_1$  as a function of the inverse of the length  $W$  of the GBJJ before (●) and after illumination (○) (adapted from Ref. 126).

for  $n = 1$  at a position  $V_L = \Phi_0 c_L / 2W$ , where  $c_L = c_0(t/\epsilon_L d)^{1/2}$  is the Swihart velocity after illumination corresponding to an effective dielectric constant  $\epsilon_L$ . One can assume that the thickness  $t$  of the weak link does not change after illumination because an increase of the Swihart velocity should indicate an increase of  $t$  and an increase of the thickness barrier would result in an increase of the normal state resistance and a decrease of the critical current, which is the opposite of the experimental results. From the experimentally observed maximum position of the Fiske resonance before and after illumination we can deduce, assuming that the barrier thickness is constant:

$$\frac{V_L}{V} = \sqrt{\frac{\epsilon}{\epsilon_L}} = 1.44, \quad (7)$$

which gives  $\epsilon_L/\epsilon \approx 0.48$ . Therefore the photodoping has an effect of decreasing continuously the relative dielectric constant up to a factor of  $\approx 2$ . This effect is related to the photodoping of the oxygen deficient barrier but the mechanism of the decrease of the dielectric constant is not well understood.

Manhart and Hilgenkamp [121] consider a more complex model of the GBJJ. They suggest that at interfaces between  $\text{YBa}_2\text{Cu}_3\text{O}_x$  and metals (or here the oxygen-depleted barrier), band bending can take place over distances of several nanometers, analogously to the band bending in standard Schotky contacts. Accordingly, depletion or accumulation layers can be formed and interfaces states have to be expected in such structures. Such interfaces states are able to turn adjacent unit cell of  $\text{YBa}_2\text{Cu}_3\text{O}_x$  into an insulator and make the GBJJ structure more complex.

## 6. CONCLUSIONS

Besides their high transition temperature ( $T_s$  up to 160 K) the HTSC show a variety of physical properties which are remarkably different from conventional superconductors and especially the PPC and PPS effects that we have described here. This is a remarkable effect of photoinduced enhancement of the superconductivity, shown by underdoped HTSC thin films. Generally, illumination can lead to a long-lived increase in doping in these materials. The most promising model to explain these effects assumes that photogenerated electrons get trapped at localized states within the charge reservoir layer.

Illumination of high-temperature superconduct-

ing thin films can be interesting because it can be used as an alternative for changing the carrier density of the  $\text{CuO}_2$  planes. This optical method has great advantages compared to other methods. With this optical method, first we keep always the same sample and furthermore the doping can be changed reversibly. Second, we do not create changes and inherent localized states in the sample structure created usually by other methods like chemical doping or physical doping such as atom or ion bombardment. Changing the photon energies of the excitation we may be able to generate electrons and holes at different energy levels.

More insight in the phase diagram relating the superconducting properties versus carrier concentration can be obtained with these illumination experiments. Starting from an underdoped sample, illumination will normally improve the superconducting properties if we stay in the underdoped regime. But starting in the overdoped regime, illumination will decrease the superconducting properties. The majority of the experiments have been done in the underdoped regime.

Recent experiments showed that persistent photoconductivity is not limited to  $\text{RBa}_2\text{Cu}_3\text{O}_x$ , but can also be observed in a variety of other high-temperature superconductors. This should encourage further experiments with other materials. In particular, persistent photoconductivity might exist in similar complex materials besides the high- $T_c$  cuprates and allows studying doping dependencies. For example, one could expect to find a photoinduced transition from an insulating antiferromagnet to a metallic ferromagnet in the colossal magnetoresistive manganites [127]. Furthermore the PPC may allow the development of novel devices. Recently Decca *et al.* [128] used an optical near-field probe to write 50-nm wide superconducting wires into an oxygen deficient  $\text{GdBa}_2\text{Cu}_3\text{O}_{6.5}$  thin film.

On the other hand, care must be taken for experiments on high temperature superconducting thin films using optical probes such as Raman scattering or photoemission spectroscopy. Indeed, Raman scattering experiments on  $\text{YBa}_2\text{Cu}_3\text{O}_{6.4}$  showed, after prolonged illumination, an increase in intensity for several phonon modes located in the  $\text{CuO}_2$  planes and the  $\text{CuO}$  chains, an increase in electronic Raman scattering at low frequencies and a suppression of the two magnon band [76]. All these effects are probably caused by the increase of the carrier density due to photodoping.

The  $\text{YBa}_2\text{Cu}_3\text{O}_x$  GBJJ with its oxygen deficient

barrier shows also these effects of PPC and PPS. Thus illumination can be used to change the Josephson coupling of  $\text{YBa}_2\text{Cu}_3\text{O}_x$  GBJJ. These effects can be interesting for adjustment of the same critical current in each junction of a dc SQUID. Optically controllable superconducting GBJJ or devices using PPS and IR quenching have been also suggested [88].

## ACKNOWLEDGMENTS

This work was supported by the U.S. National Science Foundation. We would like to thank P. Prieto and P. Seidel for useful discussions during the preparation of this review.

## REFERENCES

1. L. R. Testardi, *Phys. Rev. B* **4**, 2189 (1971).
2. W. H. Parker, *Phys. Rev. B* **12**, 3667 (1975).
3. For a review of nonequilibrium superconductivity see: *Nonequilibrium Superconductivity, Phonons and Kapitza Boundaries*, NATO Advanced Study Institute Series, K. E. Gray ed. (Plenum Press, New York, 1981).
4. D. N. Langenberg, in *Proceedings of the 14th International Conference on Low Temperature Physics*, M. Krusius and M. Vuorio, eds. (North-Holland, Amsterdam, The Netherlands, 1975), p. 223.
5. K. E. Gray, A. R. Long, and C. J. Adkins, *Philos. Mag.* **20**, 273 (1969).
6. I. Schuller and K. E. Gray, *Phys. Rev. Lett.* **36**, 429 (1976).
7. I. Schuller and K. E. Gray, *Solid State Commun.* **23**, 337 (1977).
8. S. B. Kaplan, C. C. Chi, D. N. Langenberg, J. J. Chang, S. Jaffarey, and D. Scalapino, *Phys. Rev. B* **14**, 4854 (1976).
9. C. S. Owen and D. J. Scalapino, *Phys. Rev. Lett.* **28**, 1559 (1972).
10. A. Gilbert, *Ann. Phys. (Paris)* **15**, 255 (1990).
11. J. G. Bednorz and K. A. Müller, *Z. Phys. B* **64**, 189 (1986).
12. Z. M. Zhang and A. Frenkel, *J. Supercond.* **7**, 871 (1994).
13. T. Gong, L. X. Zheng, W. Xiong, W. Kula, Y. Kostoulas, R. Sobolewski, and P. M. Fauchet, *Phys. Rev. B* **47**, 14495 (1993).
14. G. L. Eesley, J. Heremans, M. S. Meyer, G. L. Doll, and S. H. Liou, *Phys. Rev. Lett.* **65**, 3445 (1990).
15. G. L. Eesley, J. Heremans, M. S. Meyer, and G. L. Doll, *Phys. Rev. Lett.* **67**, 1054 (1991).
16. L. Shi, G. L. Huang, C. Lehane, J. P. Zheng, and H. S. Kwok, *Appl. Phys. Lett.* **61**, 489 (1992).
17. G. Yu, C. H. Lee, A. J. Heeger, N. Herron, and E. M. McCarron, *Phys. Rev. Lett.* **67**, 2581 (1991).
18. A. I. Kirilyuk, N. M. Kreines, and V. I. Kudinov, *JETP Lett.* **52**, 49 (1990).
19. V. I. Kudinov, A. I. Kirilyuk, N. M. Kreines, R. Laiho, and E. Lähderanta, *Phys. Lett. A* **151**, 358 (1990).
20. G. Nieva, E. Osquiguil, J. Guimpel, M. Maenhoudt, B. Wuyts, Y. Bruynseraede, M. B. Maple, and I. K. Schuller, *Appl. Phys. Lett.* **60**, 2159 (1992).
21. K. Tanabe, F. Hosseini-Teherani, S. Kubo, H. Asano, and M. Suzuki, *J. Appl. Phys.* **76**, 3679 (1994).
22. J. Elly, M. G. Medici, A. Gilbert, F. Schmidl, P. Seidel, A. Hoffmann, and I. K. Schuller, *Phys. Rev. B* **56**, 8507 (1997).
23. I. Giaever and H. R. Zeller, *J. Vac. Sci. Technol.* **6**, 502 (1969).

24. M. Russo, *Phys. Lett. A* **61**, 191 (1977).
25. A. Barone and M. Russo, *Phys. Lett. A* **49**, 45 (1974).
26. R. E. Somekh and Z. H. Barber, in *Physics and Material Science of High Temperature Superconductors II, Proceedings of the NATO Advanced Study Institute, Porto Carras, Greece, 18–31 Aug. 1991*, R. Kossowsky, B. Raveau, D. Wohlleben, and S. K. Patapis, eds. (Kluwer Academic Publishers, Dordrecht, The Netherlands, 1992), p. 443.
27. E. Osquiguil, M. Maenhoudt, B. Wuyts, and Y. Bruynseraede, *Appl. Phys. Lett.* **60**, 1627 (1992).
28. R. J. Cava, B. Batlogg, K. M. Rabe, E. A. Rietman, P. K. Gallagher, and L. W. Rupp, *Physica C* **156**, 523 (1988).
29. J. D. Jorgensen, B. W. Veal, A. P. Paulikas, L. J. Nowicki, G. W. Crabtree, H. Claus, and W. K. Kwok, *Phys. Rev. B* **41**, 1863 (1990).
30. R. J. Cava, A. W. Hewat, E. A. Hewat, B. Batlogg, M. Marczio, K. M. Rabe, J. J. Krajewski, W. F. Peck Jr., and L. W. Rupp Jr., *Physica C* **165**, 419 (1990).
31. J. Elly, M. G. Medici, A. Gilabert, F. Schmidl, and P. Seidel, *Physica C* **251**, 171 (1995).
32. J. Elly, *Ph.D. thesis*, University of Nice, France (1997).
33. A. Gilabert, A. Hoffmann, J. Elly, M. G. Medici, P. Seidel, F. Schmidl, and I. K. Schuller, *J. Low Temp. Phys.* **106**, 255 (1997).
34. T. Endo, A. Hoffmann, J. Santamaria, and I. K. Schuller, *Phys. Rev. B* **54**, 3750 (1996).
35. Y. Q. Shen, T. Freltoft, and P. Vase, *Appl. Phys. Lett.* **59**, 1365 (1991).
36. V. I. Kudinov, I. L. Chaplygin, A. I. Kirilyuk, N. M. Kreines, R. Laiho, and E. Lähderanta, *Phys. Lett. A* **157**, 290 (1991).
37. V. I. Kudinov, I. L. Chaplygin, A. I. Kirilyuk, N. M. Kreines, R. Laiho, and E. Lähderanta, *Physica C* **185–189**, 751 (1991).
38. V. I. Kudinov, I. L. Chaplygin, A. I. Kirilyuk, and N. M. Kreines, *Physica C* **185–189**, 1241 (1991).
39. N. M. Kreines and V. I. Kudinov, *Mod. Phys. Lett. B* **6**, 289 (1992).
40. V. I. Kudinov, *Physica B* **194**, 1963 (1994).
41. G. Nieva, E. Osquiguil, J. Guimpel, M. Maenhoudt, B. Wuyts, Y. Bruynseraede, M. B. Maple, and I. K. Schuller, *Phys. Rev. B* **46**, 14249 (1992).
42. K. Tanabe, S. Kubo, F. Hosseini-Teherani, H. Asano, and M. Suzuki, *Jpn. J. Appl. Phys.* **32**, L264 (1993).
43. N. Tyutyundzhiev and Kanev, *J. Supercond.* **6**, 179 (1993).
44. I. V. Kityk and M. I. Kolinko, *Phys. Status Solidi B* **185**, 429 (1994).
45. W. Gob, W. Lang, W. Markowitsch, C. Stockinger, W. Kula, and R. Sobolewski, in *Applied Superconductivity 1995. Proceedings of EUCAS 1995, the Second European Conference on Applied Superconductivity*, vol. 2, D. Dew-Hughes, ed. (IOP, Bristol, UK, 1995), p. 975.
46. W. Gob, W. Lang, W. Markowitsch, V. Schlosser, W. Kula, and R. Sobolewski, *Solid State Commun.* **96**, 431 (1995).
47. A. Hoffmann, J. Hasen, D. Lederman, T. Endo, Y. Bruynseraede, and I. K. Schuller, *J. Alloys Comp.* **251**, 87 (1997).
48. A. Hoffmann, D. Reznik, and I. K. Schuller, *Adv. Mat.* **9**, 271 (1997).
49. J. Hasen, *Ph.D. thesis*, University of California, San Diego (1995).
50. J. Hasen, D. Lederman, I. K. Schuller, V. Kudinov, M. Maenhoudt, and Y. Bruynseraede, *Phys. Rev. B* **51**, 1342 (1995).
51. K. Widder, J. Münzel, M. Göppert, D. Lüerssen, R. Becker, A. Dinger, H. P. Geserich, C. Klingshirn, M. Kläser, G. Müller-Vogt, J. Geerk, and V. M. Burlakov, *Physica C* **300**, 115 (1998).
52. V. I. Kudinov, A. I. Kirilyuk, and N. M. Kreines, *JETP Lett.* **56**, 102 (1992).
53. V. I. Kudinov, I. L. Chaplygin, A. I. Kirilyuk, N. M. Kreines, R. Laiho, E. Lähderanta, and C. Ayache, *Phys. Rev. B* **47**, 9017 (1993).
54. V. I. Kudinov and N. M. Kreines, *Physica B* **194–196**, 1189 (1994).
55. C. Stockinger, W. Markowitsch, W. Gob, W. Lang, W. Kula, and R. Sobolewski, in *Applied Superconductivity 1995. Proceedings of EUCAS 1995, the Second European Conference on Applied Superconductivity*, vol. 2, D. Dew-Hughes, ed. (IOP, Bristol, UK, 1995), p. 975.
56. W. Markowitsch, C. Stockinger, W. Gob, W. Lang, W. Kula, and R. Sobolewski, *Physica C* **265**, 187 (1996).
57. S. K. Tolpygo, J.-Y. Lin, M. Gurvitch, S. Y. Hou, and J. M. Phillips, *Phys. Rev. B* **53**, 12462 (1996).
58. D. Girata, B. Arenas, R. Hoyos, J. Osorio, M. E. Gomez, J. Heiras, and P. Prieto, *Physica C* **282–287**, 671 (1997).
59. E. Osquiguil, M. Maenhoudt, B. Wuyts, Y. Bruynseraede, D. Lederman, G. Nieva, J. Guimpel, and I. K. Schuller, *J. Alloys Comp.* **195**, 667 (1993).
60. K. Tanabe, S. Kubo, F. Hosseini-Teherani, H. Asano, and M. Suzuki, *Phys. Rev. Lett.* **72**, 1537 (1994).
61. C. Stockinger, W. Markowitsch, W. Lang, W. Kula, and R. Sobolewski, *J. Low Temp. Phys.* **105**, 1403 (1996).
62. R. Sobolewski, R. Adam, W. Kula, W. Markowitsch, C. Stockinger, W. Gob, and W. Lang, *IEEE Trans. Appl. Supercon.* **7**, 1632 (1997).
63. C. Stockinger, W. Markowitsch, W. Lang, W. Kula, and R. Sobolewski, *Phys. Rev. B* **57**, 8702 (1998).
64. C. Stockinger, W. Markowitsch, W. Lang, W. Kula, and R. Sobolewski, *Europ. Phys. J. B* **2**, 301 (1998).
65. V. M. Dmitriev, V. V. Eremenko, V. G. Piryatinskaya, O. R. Prikhod'ko, and E. V. Khristenko, *Sov. J. Low Temp. Phys.* **19**, 1364 (1993).
66. V. M. Dmitriev, V. V. Eremenko, I. S. Kachur, E. V. Khristenko, and O. R. Prikhod'ko, in *Proceedings of the 7th International Workshop on Critical Currents in Superconductors*, H. W. Weber, ed. (World Scientific, Singapore, 1994), p. 343.
67. V. Eremenko, V. Formin, I. Kachur, V. Piryatinskaya, and O. Prikhod'ko, *J. Appl. Phys.* **75**, 6744 (1994).
68. V. M. Dmitriev, V. V. Eremenko, I. S. Kachur, E. V. Khristenko, V. G. Piryatinskaya, O. R. Prikhod'ko, and V. V. Shapiro, *Physica C* **235–240**, 3015 (1994).
69. V. V. Eremenko, I. S. Kachur, V. G. Piryatinskaya, A. M. Ratner, and V. V. Shapiro, *Physica C* **262**, 54 (1996).
70. V. V. Eremenko, I. S. Kachur, V. G. Piryatinskaya, A. M. Ratner, and V. V. Shapiro, *Fiz. Nizk. Temp.* **23**, 146 (1997) [*Low Temp. Phys.* **23**, 106 (1997)].
71. W. Markowitsch, C. Stockinger, W. Lang, K. Bierleutgeb, J. D. Pedarnig, and D. Bäuerle, *Appl. Phys. Lett.* **71**, 1246 (1997).
72. S. Chakravarty, A. Sudbø, P. W. Anderson, S. Strong, *Science* **261**, 337 (1993).
73. J.-P. Locquet, J. Perret, J. Fompeyrine, E. Machler, J. W. Seo, and G. Van Tendeloo, *Nature (London)* **394**, 453 (1998).
74. D. Lederman, J. Hasen, I. K. Schuller, E. Osquiguil, and Y. Bruynseraede, *Appl. Phys. Lett.* **64**, 652 (1994).
75. H. Minami, M. Ishibashi, K. Oshima, and H. Uwe, in *Advances in Superconductivity VII. Proceedings of the 7th International Symposium on Superconductivity (ISS'94)*, vol. 1, K. Yamafuji and T. Morishita, eds. (Springer Verlag, Tokyo, Japan, 1995), p. 141.
76. J. Watte, G. Els, C. Andrzelak, G. Güntherodt, V. V. Moshchalkov, B. Wuyts, M. Maenhoudt, E. Osquiguil, R. E. Silverans, and Y. Bruynseraede, *J. Supercond.* **7**, 131 (1994).
77. M. Käll, M. Osada, M. Kakihamo, L. Börjesson, T. Frello, J. Madsen, N. H. Andersen, R. Liang, P. Dosanjh, and W. N. Hardy, *Phys. Rev. B* **57**, 14072 (1998).
78. M. Käll, M. Osada, J. Backstrom, M. Kakihamo, L. Börjesson, T. Frello, J. Madsen, N. H. Andersen, R. Liang, P. Dosanjh, and W. N. Hardy, *J. Phys. Chem. Solids* **59**, 1988 (1998).
79. A. Fainstein, P. Etchegoin, and J. Guimpel, *Phys. Rev. B* **58**, 9433 (1998).

80. A. G. Panfilov, A. I. Rykov, S. Tajima, and A. Yamanaka, *Phys. Rev. B* **58**, 12459 (1998).
81. T. A. Tyson, J. F. Federici, D. Chew, A. R. Bishop, L. Furenli, W. Savin, and W. Wilber, *Physica C* **292**, 163 (1997).
82. C. Ayache, I. L. Chaplygin, A. I. Kirilyuk, N. M. Kreines, and V. I. Kudinov, *Solid State Commun.* **81**, 41 (1992).
83. S. L. Bud'ko, H. H. Feng, M. F. Davis, J. C. Wolfe, and P. H. Hor, *Phys. Rev. B* **48**, 16707 (1993).
84. K. Tanabe, S. Kubo, and M. Suzuki, in *Advances in Superconductivity VII. Proceedings of the 7th International Symposium on Superconductivity (ISS'94)*, Vol. 1, K. Yamafuji and T. Morishita, eds. (Springer Verlag, Tokyo, Japan, 1995), p. 181.
85. W. Markowitsch, C. Stockinger, W. Lang, W. Kula, and R. Sobolewski, *Proc. SPIE* **2696**, 617 (1996).
86. T. Endo, J. Santamaria, A. Hoffmann, and I. K. Schuller, *Czech. J. Phys.* **46**, 1123 (1996).
87. M. K. Kelly, P. Barbois, J.-M. Tarascon, D. Aspnes, W. A. Bonner, and P. A. Morris, *Phys. Rev. B* **38**, 870 (1988).
88. M. Jiménez de Castro and J. L. Alvarez-Rivas, *Phys. Rev. B* **53**, 8614 (1996).
89. D. C. Chew, J. F. Federici, J. Gutierrez-Solana, G. Molina, W. Savin, and W. Wilber, *Appl. Phys. Lett.* **69**, 3260 (1996).
90. D. C. Chew, J. F. Federici, J. Gutierrez-Solana, G. Molina, W. Savin, and W. Wilber, *Proc. SPIE* **2696**, 654 (1996).
91. T. R. Tsai, C. L. Lin, J. L. Lin, S. S. Pai, D. H. Chen, C. C. Chi, and M. K. Wu, *Chin. J. Phys.* **34**, 616 (1996).
92. C. L. Lin, Y. K. Lin, C. C. Chi, W. Y. Guan, and M. K. Wu, *Appl. Phys. Lett.* **71**, 3284 (1997).
93. A. Hoffmann, I. K. Schuller, Z. F. Ren, J. Y. Lao, and J. H. Wang, *Phys. Rev. B* **56**, 13742 (1997).
94. B. W. Veal, H. You, A. P. Paulikas, H. Shi, Y. Fang, and J. W. Downey, *Phys. Rev. B* **42**, 4770 (1990).
95. J. D. Jorgensen, S. Pei, P. Lightfoot, H. Shi, A. P. Paulikas, and B. W. Veal, *Physica C* **167**, 571 (1990).
96. A. K. Klehe, C. Looney, J. S. Schilling, H. Takahashi, N. Mori, Y. Shimakawa, Y. Kubo, T. Manako, S. Doyle, and A. M. Hermann, *Physica C* **257**, 105 (1996).
97. E. Osquiguil, M. Maenhoudt, B. Wuyts, Y. Bruynseraede, D. Lederman, and I. K. Schuller, *Phys. Rev. B* **49**, 3675 (1994).
98. J. P. Müller, A. Schmalstieg, B. Güttler, A. Schönhals, J. Schubert, W. Zander, and H. U. Müller, *Physica C* **261**, 269 (1996).
99. J. Guimpel, B. Maiorov, E. Osquiguil, G. Nieva, and F. Pardo, *Phys. Rev. B* **56**, 3552 (1997).
100. J. F. Federici, D. Chew, B. Welker, W. Savin, J. Gutierrez-Solana, T. Fink, and W. Wilber, *Phys. Rev. B* **52**, 15592 (1995).
101. C. Guosheng, S. Jiayang, L. Xigui, D. Xianqi, W. Xizhong, and Z. Jincang, *Physica C* **282-287**, 1283 (1997).
102. S. L. Cooper, A. L. Kotz, M. A. Karlow, M. V. Klein, W. C. Lee, J. Giapintzakis, and D. M. Ginsberg, *Phys. Rev. B* **45**, 2549 (1992).
103. H. Szymczak, M. Baran, S. L. Gnatchenko, R. Szymczak, Y. F. Chen, Z. G. Ivanov, and L.-G. Johansson, *Europhys. Lett.* **35**, 452 (1996).
104. M. Maenhoudt, *Ph.D. thesis*, Katholieke Universiteit, Leuven, Belgium (1995).
105. K. Tanabe, S. Karimoto, S. Kubo, K. Tsuru, and M. Suzuki, *Phys. Rev. B* **52**, 13152 (1995).
106. A. Hoffmann, Z. F. Ren, J. Y. Lao, J. H. Wang, D. Girata, W. Lopera, P. Prieto, and I. K. Schuller, in *Applications of Spectroscopy to Superconducting Materials*, E. Faulques, ed. (ACS Books, New York, in press).
107. D. Girata, W. Lopera, P. Prieto, A. Hoffmann, and I. K. Schuller (unpublished).
108. A. Hoffmann, Y. Jaccard, I. K. Schuller, J. Perret, and J.-P. Locquet (unpublished).
109. J. Rossat Mignot, L. P. Regnault, P. Bourges, P. Burllet, C. Vettier, and J. Y. Henry, *Physica B* **192**, 109 (1993).
110. I. P. Krylov, *JETP Lett.* **52**, 442 (1990).
111. V. I. Kudinov, *Physica B* **194-196**, 1187 (1994).
112. J. L. Wagner, O. Chmaissem, J. D. Jorgensen, D. G. Hinks, P. G. Radaelli, B. A. Hunter, and W. R. Jensen, *Physica C* **277**, 170 (1997).
113. B. Beschoten, S. Sadewasser, G. Güntherodt, and C. Quitmann, *Phys. Rev. Lett.* **77**, 1837 (1996).
114. K. Tanabe, S. Kubo, F. H. Teherani, H. Asano, and M. Suzuki, *Physica C* **235-240**, 1063 (1994).
115. A. Hoffmann, I. K. Schuller, A. Gilbert, M. G. Medici, F. Schmidl, and P. Seidel, *Appl. Phys. Lett.* **70**, 2461 (1997).
116. O. M. Frölich, H. Schulze, R. Gross, A. Beck, and L. Alff, *Phys. Rev. B* **50**, 13894 (1994).
117. J. Elly, M. G. Medici, A. Gilbert, F. Schmidl, T. Schmauder, E. Heinz, and P. Seidel, *Physica C* **251**, 171 (1995).
118. J. Osoria and P. Prieto (unpublished).
119. A. Gilbert, A. Plecenik, M. G. Medici, M. Grajcar, K. Karlovsky, and R. Dittman (unpublished).
120. A. Gilbert, M. G. Medici, F. Schmidl, P. Seidel, A. Hoffmann, and I. K. Schuller (unpublished).
121. J. Manhart and H. Hilgenkamp, *Supercond. Sci. Technol.* **10**, 880 (1997).
122. D. Winkler, Y. M. Zhang, P. A. Nilson, E. A. Stepantsov, and T. Claeson, *Phys. Rev. Lett.* **72**, 1260 (1995).
123. A. Barone and G. Paterno, *Physics and Applications of the Josephson Effect*. (John Wiley & Sons, New York, 1982).
124. M. G. Medici, J. Elly, A. Gilbert, F. Schmidl, T. Schmauder, E. Heinz, and P. Seidel, in *Applied Superconductivity 1995. Proceedings of EUCAS 1995, the Second European Conference on Applied Superconductivity*, Vol. 2, D. Dew-Hughes, ed. (IOP, Bristol, UK, 1995), p. 1331.
125. E. J. Tarte, F. Baudenbacher, J. Santiso, R. E. Somekh, G. A. Wagner, and J. E. Evetts, in *Applied Superconductivity 1995. Proceedings of EUCAS 1995, the Second European Conference on Applied Superconductivity*, Vol. 2, D. Dew-Hughes, ed. (IOP, Bristol, UK, 1995), p. 1291.
126. M. G. Medici, M. Razani, A. Gilbert, A. Hoffmann, I. K. Schuller, F. Schmidl, and P. Seidel, *J. Supercond.* **11**, 225 (1998).
127. V. Kiryukhin, D. Casa, J. P. Hill, B. Keimer, A. Vigliante, Y. Tomioka, and Y. Tokura, *Nature (London)* **386**, 813 (1997).
128. R. S. Decca, H. D. Drew, B. Maiorov, J. Guimpel, and E. Osquiguil, *Appl. Phys. Lett.* **73**, 120 (1998).